Cell Metabolism

Resource

Integrative systems analysis identifies genetic and dietary modulators of bile acid homeostasis

Graphical abstract

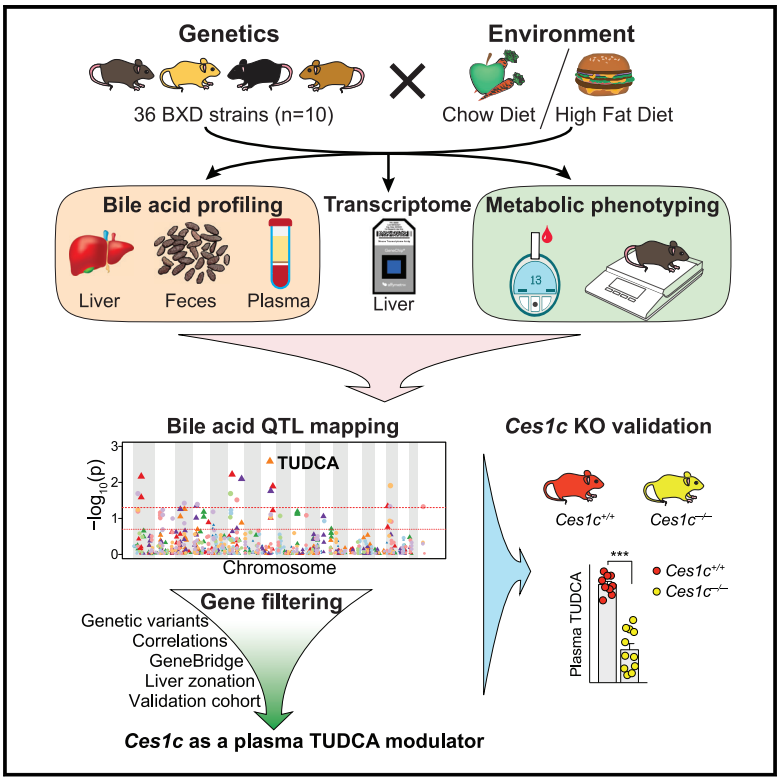

Highlights

- Multi-omics data and bile acid profiles were collected from ~360 male BXD mice
- Bile acid levels are strongly influenced by genetics and environment
- Numerous genetic loci associate to bile acid abundance
- CES1C is identified as a modulator for tauroursodeoxycholic acid plasma abundance

Authors

Hao Li, Alessia Perino, Qingyao Huang, ..., Julijana Ivanisevic, Johan Auwerx, Kristina Schoonjans

Correspondence

admin.auwerx@epfl.ch (J.A.), kristina.schoonjans@epfl.ch (K.S.)

In brief

Li et al. use the BXD mouse reference population to evaluate how genetics and diet regulate bile acid homeostasis. Through this integrated systems genetics approach, they mapped hundreds of genetic loci associated with bile acids and identified carboxylesterase 1C as a modulator for tauroursodeoxycholic acid plasma abundance.

Li et al., 2022, Cell Metabolism *34*, 1594–1610
October 4, 2022
https://doi.org/10.1016/j.cmet.2022.08.015

CellPress

CellPress
OPEN ACCESS

Cell Metabolism

Resource

Integrative systems analysis identifies genetic and dietary modulators of bile acid homeostasis

Hao Li,[1,2,5,7] Alessia Perino,[1,5] Qingyao Huang,[1,6] Giacomo V.G. Von Alvensleben,[2,6] Amir Banaei-Esfahani,[1] Laura A. Velazquez-Villegas,[1] Karim Gariani,[2] Melanie Korbelius,[1] Maroun Bou Sleiman,[2] Jéromine Imbach,[1] Yu Sun,[1] Xiaoxu Li,[2] Alexis Bachmann,[2] Ludger J.E. Goeminne,[2] Hector Gallart-Ayala,[3] Evan G. Williams,[4] Julijana Ivanisevic,[3] Johan Auwerx,[2,*] and Kristina Schoonjans[1,8,*]

[1]Laboratory of Metabolic Signaling, Institute of Bioengineering, École Polytechnique Fédérale de Lausanne, 1015 Lausanne, Switzerland
[2]Laboratory of Integrative Systems Physiology, Institute of Bioengineering, École Polytechnique Fédérale de Lausanne, 1015 Lausanne, Switzerland
[3]Metabolomics Platform, Faculty of Biology and Medicine, University of Lausanne, 1005 Lausanne, Switzerland
[4]Institute of Molecular Systems Biology, ETH Zurich, Zurich, Switzerland
[5]These authors contributed equally
[6]These authors contributed equally
[7]Present address: School of Life Science, Northwestern Polytechnical University, Xi'an 710072, China
[8]Lead contact
*Correspondence: admin.auwerx@epfl.ch (J.A.), kristina.schoonjans@epfl.ch (K.S.)
https://doi.org/10.1016/j.cmet.2022.08.015

SUMMARY

Bile acids (BAs) are complex and incompletely understood enterohepatic-derived hormones that control whole-body metabolism. Here, we profiled postprandial BAs in the liver, feces, and plasma of 360 chow- or high-fat-diet-fed BXD male mice and demonstrated that both genetics and diet strongly influence BA abundance, composition, and correlation with metabolic traits. Through an integrated systems approach, we mapped hundreds of quantitative trait loci that modulate BAs and identified both known and unknown regulators of BA homeostasis. In particular, we discovered carboxylesterase 1c (*Ces1c*) as a genetic determinant of plasma tauroursodeoxycholic acid (TUDCA), a BA species with established disease-preventing actions. The association between *Ces1c* and plasma TUDCA was validated using data from independent mouse cohorts and a *Ces1c* knockout mouse model. Collectively, our data are a unique resource to dissect the physiological importance of BAs as determinants of metabolic traits, as underscored by the identification of CES1C as a master regulator of plasma TUDCA levels.

INTRODUCTION

Bile acids (BAs), traditionally known for their role as lipid emulsifiers in the gut, have recently emerged as powerful hormones with pleiotropic beneficial effects in physiology and a major impact on multifactorial diseases (Kuipers et al., 2014; Perino et al., 2020; Schaap et al., 2014). Primary BAs, that is, cholic acid (CA) and chenodeoxycholic acid (CDCA) in humans, and CA, CDCA, and muricholic acids (αMCA and βMCA) in mice, are synthesized from cholesterol in the liver. Upon synthesis, they are conjugated with taurine (T) or glycine (G), stored in the gallbladder, and released in the intestinal lumen after food intake to facilitate lipid absorption (Kuipers et al., 2014; Perino et al., 2020). Once they reach the lower intestine, primary BAs are transformed into secondary BAs by gut bacterial enzymes (Wahlström et al., 2016). While only a minor fraction is excreted in the feces, the majority of BAs return to the liver via the portal vein and cycle between the gut and the liver through the enterohepatic circulation. During this process, some BAs spill over in the systemic circulation and reach organs other than those of the enterohepatic axis. Because of their widespread distribution during the postprandial state, BAs are considered as versatile endocrine factors integrating the nutritional status to whole-body metabolic adaptation through the coordinated activation of two well-studied BA receptors, the nuclear receptor farnesoid X receptor (FXR) and the G protein-coupled receptor TGR5 (Kuipers et al., 2014; Perino et al., 2020; Perino and Schoonjans, 2022).

Despite the crucial role of BAs on whole-body physiology, their genetic and environmental regulators remain to be fully understood. One approach to identify such regulators is to take advantage of genetic association or linkage studies in large human cohorts (Chen et al., 2020; Visscher et al., 2017). However, human studies often have difficulties in controlling confounding environmental factors and do not allow accessing relevant deep biological compartments due to ethical reasons (Li and Auwerx, 2020). An alternative approach is to use genetically diverse animal populations as simplified models to investigate the determinants of phenotypic traits (Kemis et al., 2019), as findings in such studies can then be translated into humans (Li and Auwerx,

CellPress
OPEN ACCESS

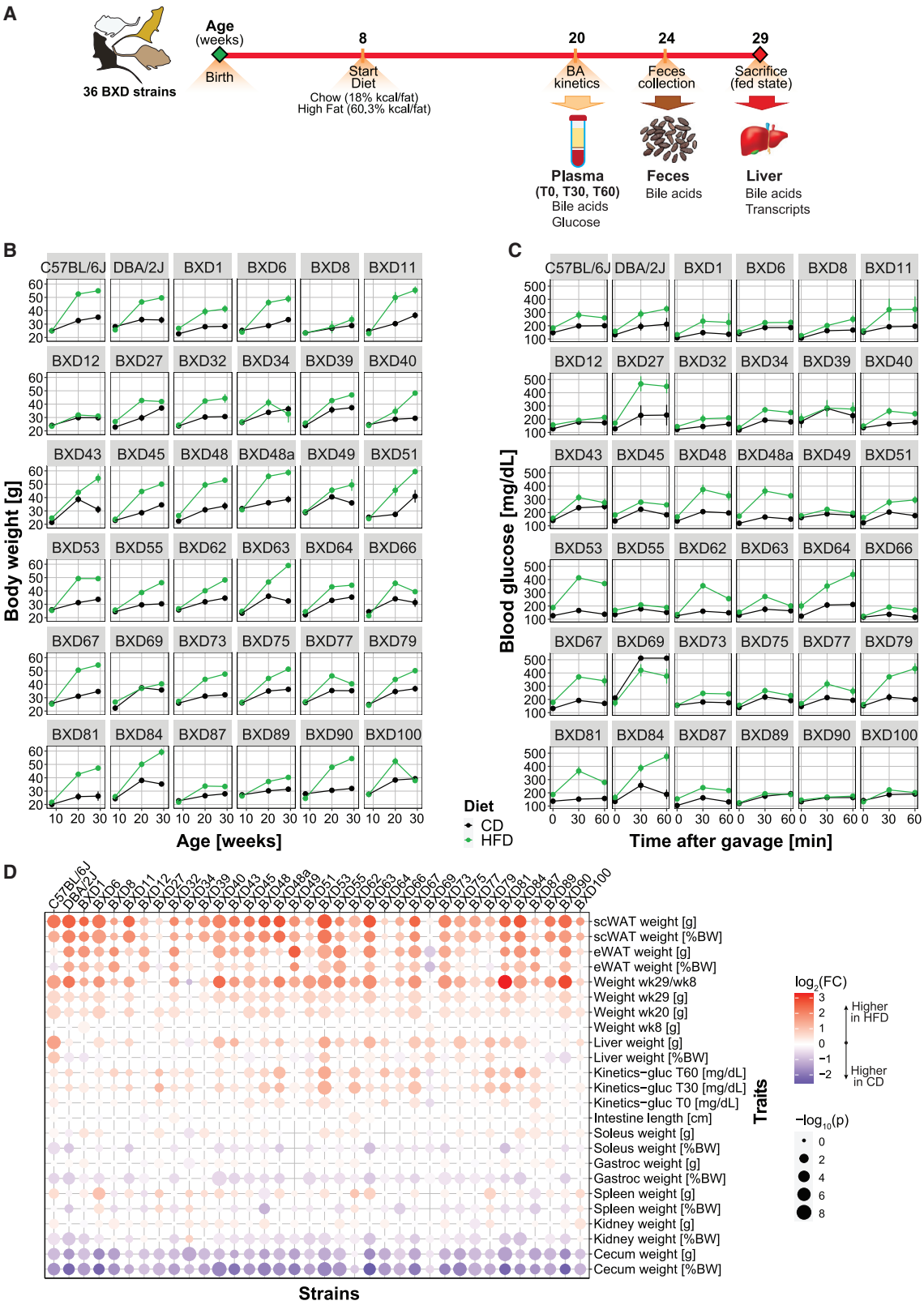

(legend on next page)

2020; Nadeau and Auwerx, 2019). Previous unbiased systems genetics approaches relying on the use of mouse genetic reference populations (GRPs) have been successful in identifying the underlying mechanisms in complex metabolic traits, such as mitochondrial function (Chella Krishnan et al., 2018; Norheim et al., 2019; Williams et al., 2016), lipid metabolism (Jha et al., 2018a, 2018b; Linke et al., 2020; Parker et al., 2019), atherosclerosis (Bennett et al., 2015; Smallwood et al., 2014), and liver diseases (Chella Krishnan et al., 2018; Hui et al., 2018).

In this study, we used 36 genetically diverse mouse strains from the BXD cohort, derived from crosses between a C57BL/6J mother and a DBA/2J father (Li et al., 2018), as the genetic model to gain insight into the determinants of BA homeostasis. Stable isotope dilution mass spectrometry was applied to quantify the postprandial abundance of 27 BA species in the liver, feces, and plasma of ~360 animals. The postprandial BA levels in the different biological compartments analyzed strongly correlated with several metabolic phenotypes that had been collected in this study and in a previous BXD cohort analyzed in our laboratory (Williams et al., 2016). Moreover, transcriptomic profiling was performed on liver samples of the same animals to assess gene expression. Systems genetics analysis integrating these omics datasets revealed hundreds of genetic loci associating with BA levels, including established regulators of BA synthesis (e.g., *Cyp8b1* and *Cyp7b1*) (Li-Hawkins et al., 2002; Li-Hawkins et al., 2000) and transport (e.g., *Abcb11*) (Gerloff et al., 1998), as well as newly identified BA modulators. In particular, we identified CES1C as a novel modulator of tauroursodeoxycholic acid (TUDCA) plasma abundance through an integrative systems genetics approach. TUDCA is known to trigger multiple health-promoting actions and is widely established as a therapeutically relevant target for various pathologies (Kusaczuk, 2019). The association between the *Ces1c* locus and plasma TUDCA levels was validated using data from independent mouse diversity outbred (DO) (Chick et al., 2016; Kemis et al., 2019) and CC cohorts (Keele et al., 2021) and further confirmed using a *Ces1c* loss-of-function mouse model. Our study thus provides new insight into the genetic and environmental regulation of BA homeostasis and highlights the significance of the integrative systems approach in the investigation of complex traits and diseases.

RESULTS

Multi-omics profiling to study the postprandial BAs in the BXD cohort

To study the genetic and environmental determinants that link BAs to metabolic homeostasis, we designed an experimental pipeline using 36 strains of the BXD mouse GRP to profile metabolic parameters and collect relevant biological material for multi-omics measurements, including BAs (Figure 1A). In total, about 360 male mice (~10 for each strain) were fed with either a regular chow diet (CD) or a high-fat diet (HFD) to induce obesity and associated metabolic stress. At 20 weeks of age, a test meal bolus was administered orally, and postprandial BAs and blood glucose levels were analyzed at three different time points (before and 30 or 60 min after gavage). Nine weeks later, the mice were sacrificed 4 h after feeding, a time point in which the main metabolic adaptive processes in response to BA-mediated food intake are captured. The BXD strains vary in metabolic performance, as illustrated by the differences in body weight (Figure 1B) and blood glucose levels after a test meal gavage (Figure 1C). As expected, for most of the strains, HFD feeding significantly increased body weight, fat mass, and blood glucose levels (Figures 1B–1D), while no effect or even a decrease was observed in small intestine length and cecum weight, respectively (Figure 1D). Moreover, the changes in particular metabolic traits to the HFD challenge showed clear differences across strains (Figure 1D), suggesting the involvement of gene-environment interactions (GXEs). For example, BXD8 and BXD12 showed no obvious weight gain under HFD feeding compared with CD, while BXD81 and BXD90 almost doubled their body weight (Figures 1B and 1D). In general, HFD feeding caused a significant increase in blood glucose levels after a test meal administration (Figures 1C and 1D) although this was not the case for some strains, such as BXD89, in which the glycemia was comparable in the two diets, despite the body weight difference (Figures 1B–1D). Remarkably, BXD69 appeared resistant to HFD as depicted by the marginal effects on fat mass, body weight, and blood glucose levels (Figures 1B–1D), with the latter trait being high already during CD and even tending toward a reduction after HFD (Figure 1C).

In addition to these clinical phenotyping data, we biobanked liver (the main organ for BA biosynthesis) and plasma (medium for BA transport) samples in the postprandial state; feces were also collected as a proxy for primary BA bacterial transformation and primary and secondary BA excretion. Stable isotope dilution mass spectrometry was used to quantify the concentration of 27 BA species in the postprandial liver (4 h after feeding), feces (collection over a period of 24h), and plasma (before and 30 or 60 min after a test meal, indicated as T0, T30, and T60, respectively) (Tables S1 and S2). We quantified the abundance of around 20,000 transcripts in the liver samples by microarray and integrated these data with the BA measurements and metabolic traits, as well as the genotypes to identify modulators of BA homeostasis.

Figure 1. Metabolic phenotyping of the BXD-BA study

(A) Phenotyping pipeline of the BXD-BA study that included 36 BXD strains. 8-week-old male mice were fed with either chow diet (CD) or high-fat diet (HFD) (5 mice/strain/diet). Details of the clinical phenotyping protocol are described in the STAR Methods section. Plasma, feces, and liver samples were collected from the animals at indicated time points, and then BAs and transcripts were profiled from the obtained biological samples.

(B) Body weight growth curve of the animals from 36 BXD strains described in (A).

(C) Glucose levels after test meal oral administration in the 36 BXD strains described in (A).

Results in (B) and (C) are expressed as mean ± SEM.

(D) Dot plot showing the diversity in the body/tissue mass and metabolic response of each BXD strain upon HFD feeding. The dot color represents the $\log_2$ fold change (FC) of the phenotypic traits upon HFD over CD, with red indicating higher in HFD and blue indicating higher in CD, whereas the dot size represents the significance of the changes. p value was calculated using a two-tailed Student's t test. BW, body weight; gluc, blood glucose levels; wk, week; scWAT, subcutaneous white adipose tissue; eWAT, epididymal white adipose tissue; gastroc, gastrocnemius.

See also Table S2.

CellPress
OPEN ACCESS

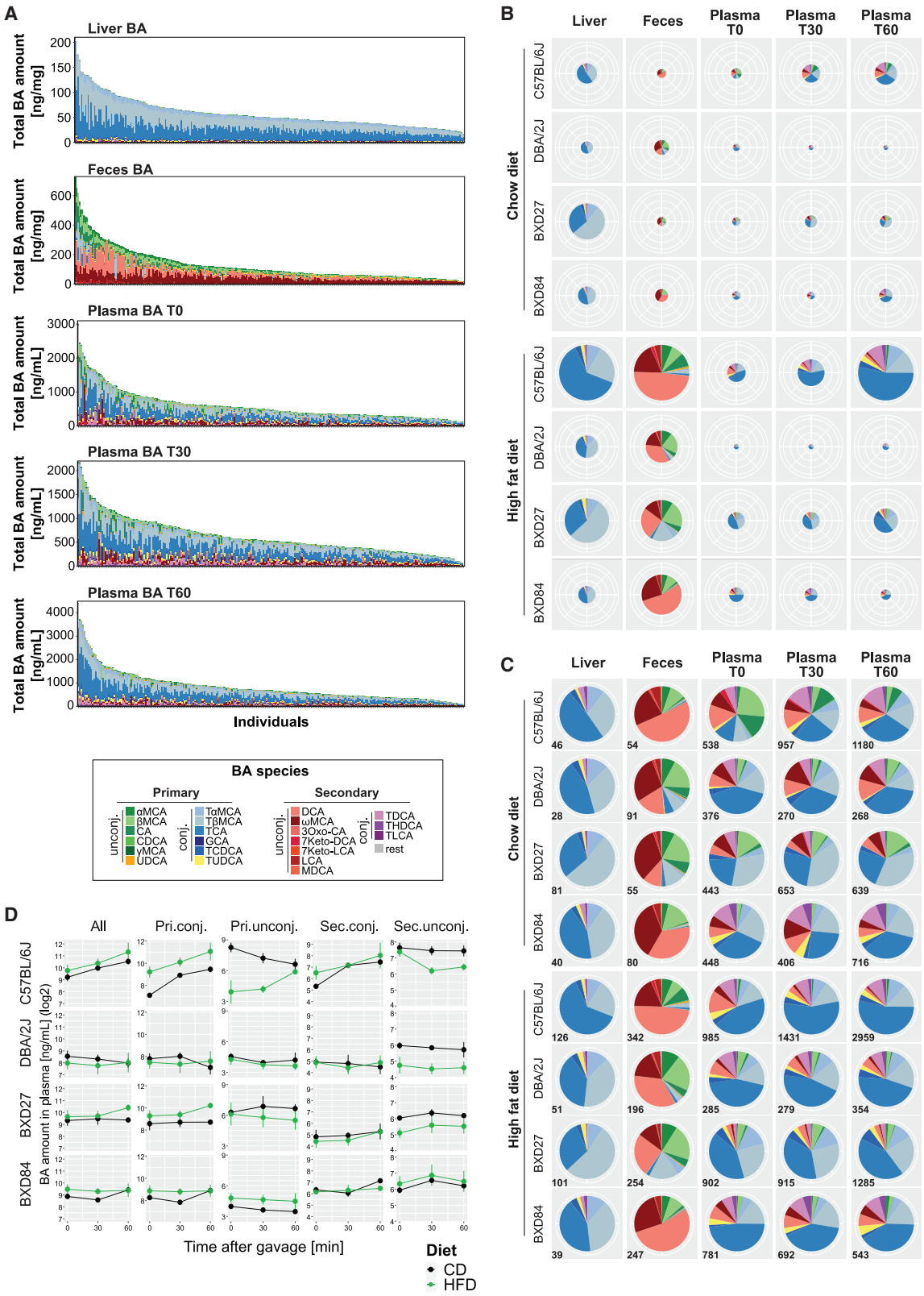

Figure 2. Diversity of BAs across strains, diets, and biological compartments

(A) Stacked barplots showing BA amount and composition in the liver, feces, and plasma (before and 30 or 60 min after gavage of a test meal) of each individual animal from different BXD strains. Animals are ranked by the BA amount in each individual compartment. The BA species are categorized and colored to highlight

(legend continued on next page)

Genetics and environment contribute to the diversity of BAs across individuals

Using these collected data, we examined the differential distribution of BA species in different biological compartments, as well as the contribution of the genetic and dietary factors. Across strains, BAs showed large differences in both their abundance (Figures 2A and S1A–S1E) and composition (Figures 2A and S1F–S1J) in the liver, feces, and plasma. When comparing the two CD-fed parental strains, C57BL/6J mice showed higher BA levels in the liver and plasma than DBA/2J mice (Figure 2B). This variability was also apparent in the BXD strains. CD-fed BXD27, for instance, displayed high BA levels in the liver but not in the feces and plasma (Figure 2B). As expected, the liver and feces behaved as distinct compartments, each composed of virtually mutually exclusive BA species, while the plasma was a hybrid of the two (Figures 2A and S1F–S1J). In particular, tauro-conjugated primary BAs (blue colors) were the main BA species in the liver, with a negligible percentage of tauro-conjugated secondary BAs (purple colors) and virtually no unconjugated primary BAs (green colors) (Figures 2A and S1F). In contrast, unconjugated BAs were the most abundant species in the feces, with a higher percentage of secondary (red colors) over primary (green colors) BAs and only marginal levels of tauro-conjugated primary BAs (Figures 2A and S1G). Of note, all BA categories were found in the plasma, with an enrichment of tauro-conjugated primary BAs and a significant amount of secondary conjugated and unconjugated BAs (Figures 2A and S1H–S1J). The BA distribution in the different biological compartments, especially in feces and plasma, was significantly affected by genetics (Figures S1F–S1J). For instance, DBA/2J and BXD27 exhibited a relatively high percentage of conjugated primary BAs in feces when compared with C57BL/6J and BXD84 (Figures 2B and 2C), indicating that differences in genetic background can be responsible for altered BA reabsorption, dysbiosis, or deconjugation.

In addition to genetics, HFD feeding significantly shaped BA abundance (Figures S1A–S1E) and composition (Figures S2A–S2E) in a strain-dependent manner (Figures 2B, 2C, and S3A–S3E). For instance, HFD raised BA levels in the liver, feces, and plasma of the C57BL/6J strain, whereas the changes in DBA/2J were only modest or undetectable (Figures 2B and S3A–S3E). Of note, the HFD-dependent increase in BA levels was more consistent in feces (Figure S1B), especially for the secondary BAs (Figure S3B), with the exception of a few strains, including BXD8 and BXD12. Remarkably, these strains were also resistant to HFD-induced metabolic dysfunction (Figures 1B and 1C). Overall, HFD feeding caused an imbalance in the relative BA levels in all biological compartments analyzed, with an increase in primary and a decrease in secondary BAs (Figures S2A–S2E). These data suggest an adaptation of BA homeostasis following chronic HFD feeding, likely resulting from the HFD-induced reduction in microbial diversity (Cani et al., 2008; David et al., 2014; Devkota et al., 2012; Hildebrandt et al., 2009; Sonnenburg and Bäckhed, 2016). HFD also significantly modified the total plasma BA levels at T0 and T60, but not at T30 ($p = 0.17$) (Figures S1C–S1E), which may point to a progressive alteration in the recycling of BAs following chronic HFD. Consistent with these findings, a negative correlation was found between fecal and plasma BA levels in CD, while in HFD, this correlation was lost (Figure S4A). On the contrary, BA levels showed a strong positive correlation in plasma in both diets at all 3 time points (Figures S4A and S4B).

Consistent with the role of BAs as a proxy of postprandial metabolism, the nutritional status also influenced plasma BA levels. Most BXD strains, including the C57BL/6J, had an increased plasma BA amount shortly after the delivery of nutrients by controlled gavage feeding, whereas in other strains, exemplified by the DBA/2J, the plasma BA amount was not changed or even decreased (Figures 2B, 2D, S5A, and S5B), suggesting strain-dependent differences in postprandial BA recycling. Gavage feeding also showed a strong impact on the BA composition, illustrated by the overall increased proportion of primary BAs in most strains, especially at 60 min after the test meal gavage (Figures S5C and S5D). Furthermore, the test meal also generally decreased the percentage of both primary (Figures S5E and S5F) and secondary (Figures S5G and S5H) unconjugated BAs. Overall, these data corroborate the striking differences in BA composition and abundance in the different biological compartments and highlight the importance of genetics and environment in regulating BA homeostasis.

Genetic background affects the BA abundance and composition in response to HFD

Next, we evaluated the influence of genetics and diet on the abundance of BA species by calculating the heritability of the BAs measured in the study. Most BAs had a heritability over 0.5, indicating a strong genetic influence (Figure 3A, black and green dots; Table S3). As expected, the heritability of BAs significantly dropped when ignoring environmental factors by mixing data from mice fed with different diets; this simulates situations where such environmental factors are not well controlled and monitored, for example, in human genetics studies (red dots in Figure 3A). The influence of genetics and diet on BA levels varied across the BA species and biological compartments (Figure 3A); for example, genetics contributed only 30% of the variance for plasma TαMCA, while the value was 90% for DCA in feces (Figures 3B [black and green bars], 3C, and S5I). The GXE effects also showed variations across BA species (yellow dots in

primary unconjugated (green and UDCA in orange), primary conjugated (blue and TUDCA in yellow), secondary unconjugated (red), and secondary conjugated (purple) BAs. The BA abbreviations are included in Table S1.

(B and C) Pie charts showing BA amount and composition in the liver, feces, and plasma of mice from C57BL/6J, DBA/2J, BXD27, and BXD84 strains fed CD or HFD. (B) The radius of pie defines the BA amount in the indicated biological compartments and pie slices define the BA composition. (C) The same BA data represented in (B) are normalized to total BA amount to increase the visibility of the BA composition. Numbers in the lower left corner of each pie chart correspond to BA amount (ng/mg for liver and feces and ng/mL for plasma).

(D) Plasma BA concentrations, stratified according to BA categories, after test meal oral administration in the four selected strains as in (B). Results are expressed as mean ± SEM. Pri.conj., primary conjugated; Pri.unconj., primary unconjugated; Sec.conj., secondary conjugated; Sec.unconj., secondary unconjugated.
See also Figures S1–S5 and Tables S1 and S2.

CellPress
OPEN ACCESS

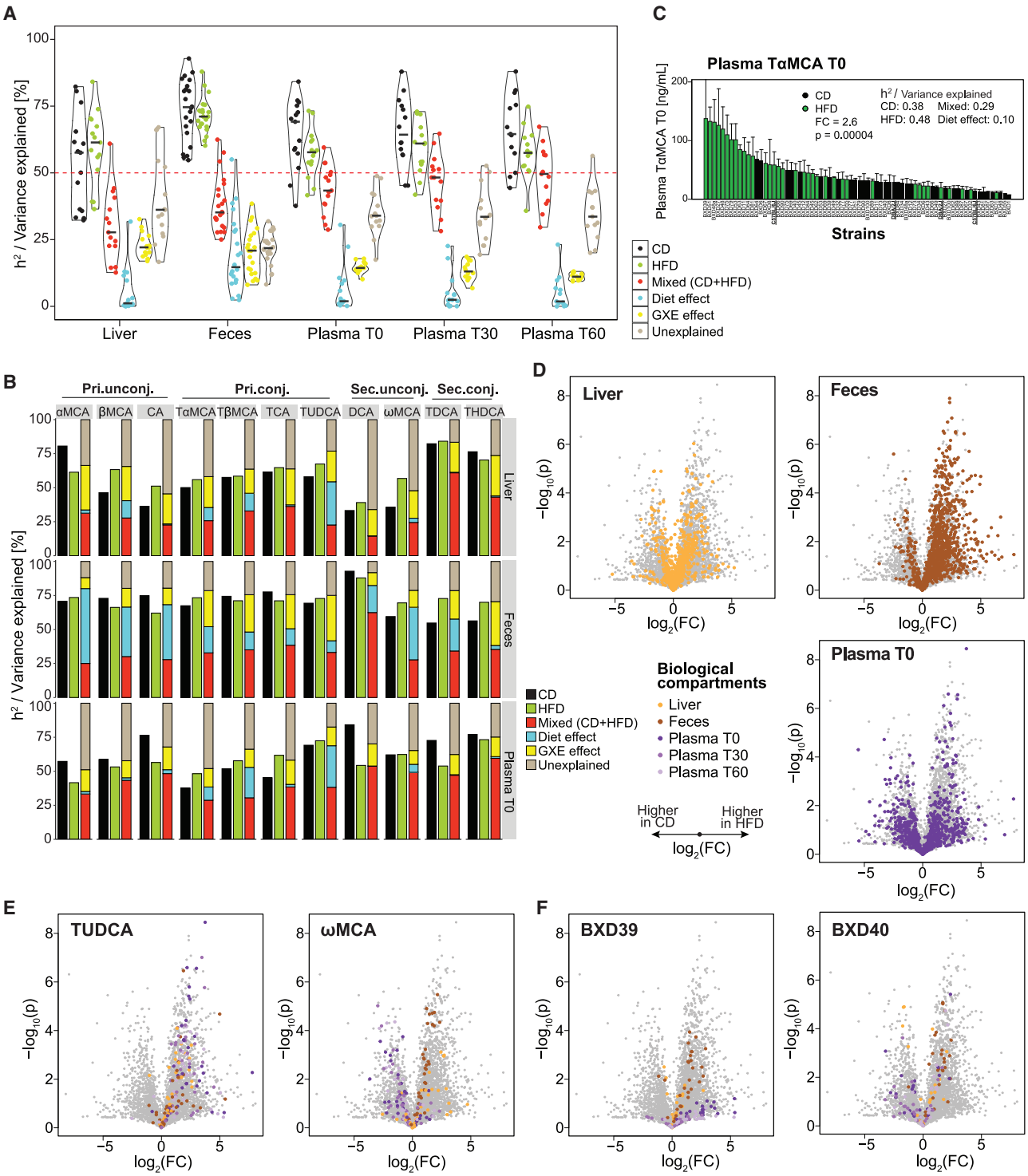

Figure 3. Postprandial BA levels are highly influenced by genetic and dietary factors

(A) The percentage of variance in individual BAs that can be explained by different factors, that is, the genetics (CD, HFD, or mixed), environment (diet), and gene-environment interaction (GXE). BAs were grouped based on the biological sources in which they were profiled. The black thick horizontal line in the violin plots shows the median variance explained for all BAs in the indicated sources. The heritability results for each individual BA are available in Table S3.

(B) Examples of BA species with distinct heritability measures explained by different factors. BAs with varying abundancies in each of the compartments were selected as examples (primary unconjugated: αMCA, βMCA, and CA; primary conjugated: TαMCA, TβMCA, TCA, and TUDCA; secondary unconjugated: DCA and ωMCA; secondary conjugated: TDCA and THDCA).

(legend continued on next page)

Figure 3A), for example, fecal DCA versus plasma ωMCA (Figures 3B [yellow bars], S5I, and S5J). A similar statement could be made for the environmental effects; diet contributed over 30% of the variance for plasma TUDCA T0 (fasting; before test meal) but had almost no contribution for hepatic TCA (Figures 3B [blue bars], S5K, and S5L). In general, we found that fecal BAs showed stronger diet effects than those measured in the liver and plasma (blue dots in Figure 3A). Indeed, HFD challenge led to an overall increase of BAs in feces but not in the liver or plasma (Figures 3D and S3A–S3E). Different BA species also exhibited a distinct response to HFD (Table S4). For example, TUDCA increased consistently after HFD challenge in all biological compartments, whereas ωMCA showed a significant increase in feces and liver but a decrease in plasma upon HFD (Figures 3E and S3A–S3E). The differences in response to HFD also applied to the different BXD strains (Figures S3A–S3E). For instance, BXD39 showed an induction in almost all BA species from all biological compartments, while BXD40 had increased BAs in feces and decreased BAs in plasma (Figure 3F). Collectively, these data demonstrate the influence of genetic and environmental factors on BAs and reveal that the response of BAs to HFD challenge is influenced by the genetic background of the strains and varies across BA species and biological compartments.

Associations between BAs and metabolic traits

By integrating BA measurements with metabolic traits, we were able to identify a large number of associations between BAs and metabolic phenotypes collected in this study and in a previous BXD cohort from our laboratory (Williams et al., 2016) (Figure 4A; Table S5). These results suggest a high correlation of the BA levels within the different biological compartments, especially in plasma, and a significant involvement of BAs in the metabolic performance of mice. For instance, the ratio of secondary BA to total BA levels negatively correlated with fat mass, food intake, and body weight, while they positively correlated with gastrocnemius and soleus muscle mass in CD (Figure 4B), which could point to a potential involvement of TGR5 (Perino et al., 2021; Sasaki et al., 2021). Of note, most of these associations were lost in HFD (Figure 4B), a condition in which most secondary BAs are decreased (Figures S3A and S3C–S3E, blue dots), indicating a significant influence of the diet on the physiological effects of BAs. As expected, opposite correlations with these phenotypes were found for the primary BA to total BA ratio (Figure 4C), suggesting a differential impact of primary versus secondary BA signaling in modulating metabolic phenotypes. Moreover, the association between BAs and metabolic phenotypes changed accordingly to the BA species. For example, while TCA levels followed the trend of primary BAs, with a positive correlation of plasma TCA with fat mass in CD and even stronger in HFD (Figure 4D), plasma tauro-β-muricholic acid (TβMCA) only showed positive correlations with fat mass and body weight in CD but not in HFD (Figure 4E). As the latter BA acts as an FXR antagonist (Sayin et al., 2013), some of these phenotypic correlations could be mediated through FXR inhibition. Previous reports have shown that 12α-hydroxylated (12α-OH) BAs promote type 2 diabetes (Haeusler et al., 2012, 2013). Interestingly, plasma, but not hepatic or fecal TCA levels (the predominant form of 12α-OH BAs), from HFD cohorts was significantly associated with insulin and glucose levels (Figure 4D). These findings further indicate that BAs can have distinct associations with traits depending on the compartment from which they were profiled.

Systems genetics analyses to unveil potential determinants of BA homeostasis

We next conducted an integrative systems approach to identify genetic mechanisms modulating BA homeostasis. Specifically, through quantitative trait locus (QTL) mapping, we identified hundreds of loci associated with BA species (Figure 5A; Table S6). Among the most significant hits, plasma TUDCA was prominently associated with a locus on chromosome 8 (Figure 5A). Moreover, the QTL for plasma TUDCA levels mapped consistently to the same locus at 80–110 Mb on chromosome 8 across different time points after feeding and in both CD- and HFD-fed animals (Figure 5B), suggesting a conserved regulatory mechanism of plasma TUDCA.

We also mapped the QTLs for the pairwise ratios between BAs within each biological compartment as previously described (Gieger et al., 2008; Shin et al., 2014) (Figure 5C). Of interest, QTL signals for plasma TUDCA on chromosome 8 became more significant when considering the ratio of TUDCA to total BA levels (Figure 5D). We further expanded the concept to estimate the BA recycling by computing the ratios of the same BA between different biological compartments in which BAs are synthesized, transported, or excreted. Many QTLs were identified in this configuration, suggesting a possible modulation of their secretion or transport (Figure 5E). For instance, we determined a significant QTL on chromosome 1 for the ratio of plasma secondary BA levels (T0; before test meal) to the liver in CD (Figure 5F). Of note, among all the different QTLs mapped in this study, we found several well-established genes involved in BA synthesis and transport, including *Cyp8b1* (Li-Hawkins et al., 2002), *Cyp7b1* (Li-Hawkins et al., 2000) (Figures 5G and S6A), and *Abcb11* (Gerloff et al., 1998) (Figure 5G). Furthermore, BAs and some metabolic traits, collected in a separate study (Williams et al., 2016), co-mapped in a number of loci (Figure 5H; Table S7). For instance, plasma secondary BAs (T0 in HFD) co-mapped with glucose levels on chromosome 17 (Figure 5I) and plasma secondary conjugated BAs and taurodeoxycholic acid (TDCA) (T60) co-mapped and correlated with respiratory exchange ratio (RER) (Figure 5J and 5K). Although these co-mappings were only

(C) Barplot showing the levels of plasma TαMCA at T0 for each BXD strain. Strains are ranked by plasma TαMCA levels. Barplot is expressed as mean + SEM. p values were calculated using paired-sample t tests between CD and HFD. Fold change (FC) was calculated based on the average of BA changes in HFD compared with CD.

(D–F) Volcano plots showing the changes of BA levels in response to a HFD challenge across different biological compartments (D), BA species (E), and BXD strains (F). The x axes show the $\log_2$ fold change (FC) of BA levels upon HFD challenge, and y axes show the significance of the changes. Several examples are shown in the figure and results for each individual BA are depicted in Table S4.

See also Figure S5 and Tables S1, S2, S3, and S4.

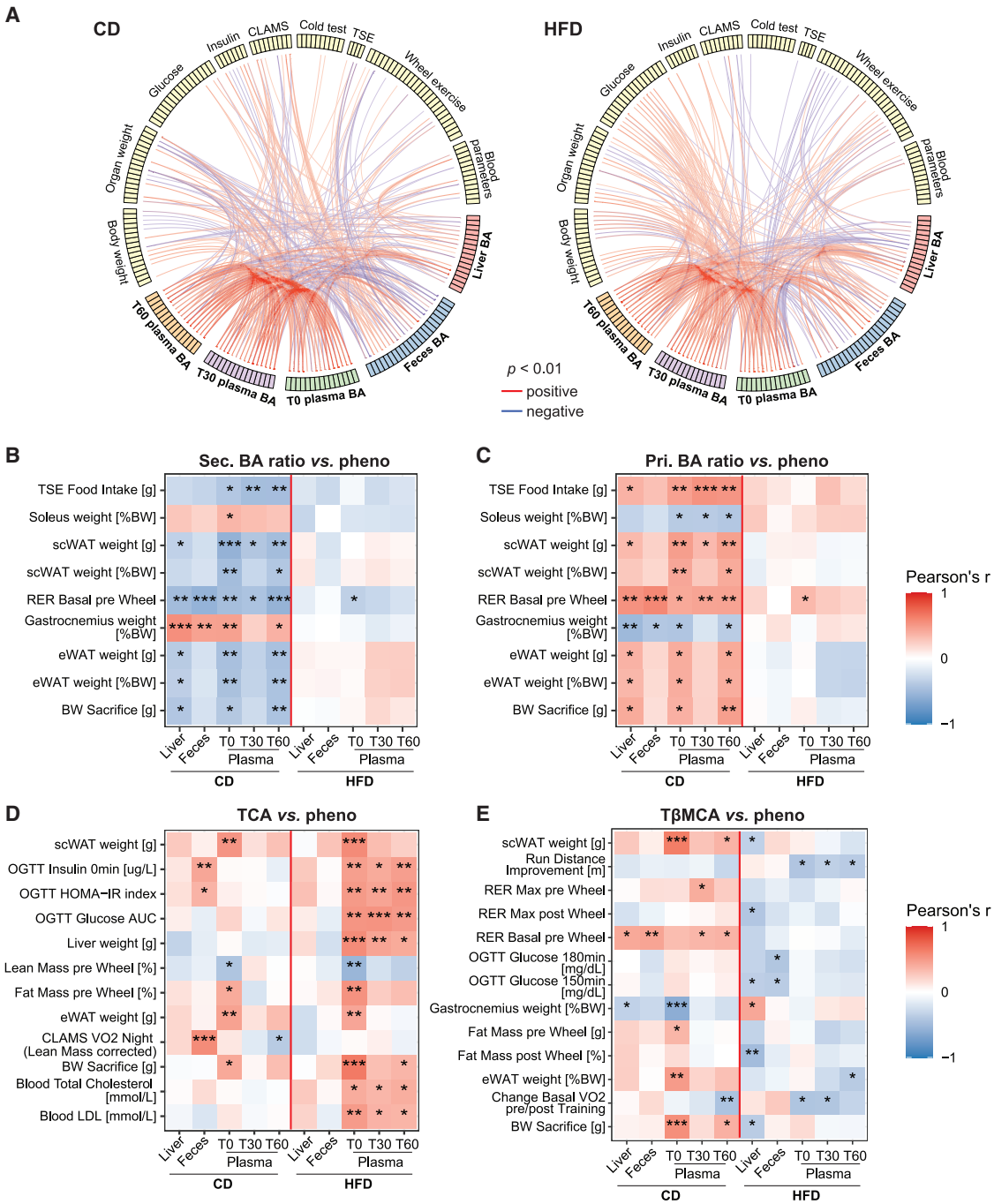

Figure 4. Associations between BA levels and metabolic traits

(A) Circos plot showing the correlations between BA amount (log_2 data) and phenotypic traits in CD (left) or HFD (right). Phenotypic traits collected from the BXD animals were manually categorized into different groups. Only BA-trait pairs with a correlation p value less than 0.01 were plotted. Colors of the connecting lines represent the correlation coefficient of the respective BA-trait pairs, with red lines and blue lines indicating positive and negative correlations, respectively.

(B–E) Heatmaps presenting the correlation between secondary BA to total BA ratio (B), primary BA to total BA ratio (C), TCA (D), or TβMCA (E) levels across biological compartments and phenotypic traits. *p < 0.05, **p < 0.01, and ***p < 0.001.

See also Tables S1, S2, and S5.

suggestive, these trends support earlier studies in which secondary BAs have been associated to various beneficial metabolic effects (Thomas et al., 2009; Velazquez-Villegas et al., 2018; Watanabe et al., 2006).

Identification of carboxylesterase 1C as a key candidate regulator of TUDCA

We next sought to identify the potential genetic determinants of plasma TUDCA, which had the most significant QTL in our

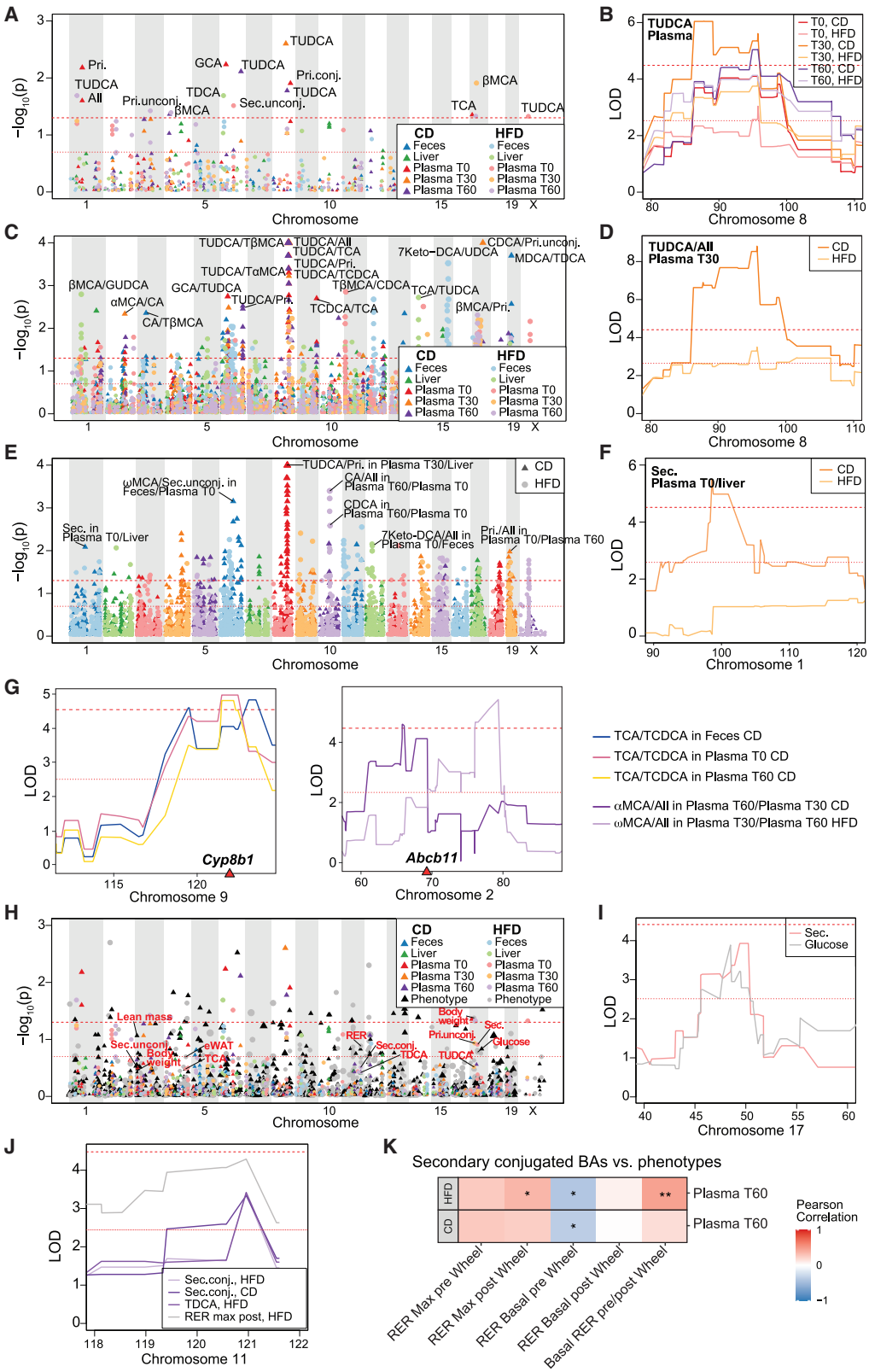

(legend on next page)

analysis (Figures 5A and 5B). BXD strains inheriting the genotype from C57BL/6J (B/B) at this QTL had much higher plasma TUDCA than those inheriting it from DBA/2J (D/D), in both CD and HFD (Figure 6A). TUDCA is also of particular interest because of its abundance in bear bile and use in traditional medicine for alleviating a wide range of diseases, including hepatobiliary, metabolic, inflammatory, cardiac, and neurological disorders (as reviewed in Cabrera et al., 2019; Kusaczuk, 2019; Qin et al., 2017; Rodrigues et al., 2003; Xia et al., 2020; Zangerolamo et al., 2021). The beneficial role of plasma TUDCA in metabolism is supported by its positive correlation with RER and negative correlation with fat mass and blood glucose (Figure 6B). TUDCA was long believed to be a secondary BA, microbially transformed from CDCA, in rodents and humans (Russell, 2003). Recent results from several studies using germ-free mice, however, indicated that TUDCA is a primary BA, at least in rodents (Marion et al., 2020; Sayin et al., 2013; Selwyn et al., 2015). The regulators of hepatic TUDCA synthesis, however, are not yet known.

Having 191 genes located in the region of the TUDCA QTL on chromosome 8, we developed an integrative systems approach to prioritize genes that are responsible for the variance of TUDCA levels in the BXD mice based on the combination of several criteria (Figure 6C). This method integrated the genetic variants and the hepatic expression levels for genes in the QTL region in the BXDs to shortlist the best candidates for further validation. GeneBridge, a systems genetics approach based on large-scale expression datasets (https://systems-genetics.org/) (Li et al., 2019), was also employed to predict the associations between the primary BA biosynthesis module and genes in this locus. We used plasma TUDCA levels at T30 for the analysis because it yielded the strongest QTL signal; however, similar results were obtained using plasma TUDCA at other time points (data not shown). Using this integrative approach, we identified 3 potential TUDCA modulators. More specifically, glutaryl-CoA dehydrogenase (*Gcdh*), carboxylesterase 1b (*Ces1b*), and carboxylesterase 1c (*Ces1c*) fulfilled all the selection criteria (Figures 6C, 6D, and S6B–S6D; Table S8) and showed enhanced expression in the liver (Figure 6D).

We leveraged single-cell RNA-sequencing (scRNA-seq) datasets of the human and mouse liver (Aizarani et al., 2019; Halpern et al., 2017) to further demonstrate that their specific expression is functionally relevant for BA synthesis and homeostasis. Of the three genes, *Ces1c* was most abundantly expressed in hepatocytes, where BAs are synthesized (Figures S6E–S6I). Recent studies demonstrated that key liver BA biosynthesis enzymes follow a spatial order (or zonation) across different hepatocyte layers and are largely enriched in the pericentral zone (Ben-Moshe et al., 2019; Halpern et al., 2017). We then explored scRNA-seq and proteomics datasets produced from spatially sorted hepatocytes to determine the zonation patterns of the 3 candidate genes. The results showed that *Ces1c* (both mRNA and protein) and *Ces1b* (mRNA) were predominantly expressed in the pericentral region, similar to the well-known BA synthesis genes (Ben-Moshe et al., 2019; Halpern et al., 2017), whereas expression of *Gcdh* was less zonated (Figure 6E). Using a recent spatial transcriptomics dataset from the mouse liver (Cho et al., 2021), we further ascertained *Ces1c* as the most prominent gene with preferable expression in the pericentral hepatocytes in this locus (Table S9). Overall, these results suggested that *Ces1c* is the most likely candidate modulator of plasma TUDCA levels.

Validating the association between *Ces1c* and TUDCA through independent mouse cohorts and a *Ces1c* knockout mouse model

To further validate the associations identified in our current study, we retrieved published BA data acquired from 384 DO mice (Kemis et al., 2019) as an independent validation cohort. Of note, we identified a significant QTL at the same locus on chromosome 8 for plasma TUDCA in the DO cohort (Figure 7A), confirming a strong and conserved genetic association between this genetic locus and plasma TUDCA. In concordance with the primary results obtained from the BXD strains (Figure 6A), DO mice inheriting C57BL/6J alleles of this locus (AA) showed significantly higher plasma TUDCA levels than those with alternative alleles (aa) (Figure 7B). To unravel the genes responsible for the modulation of plasma TUDCA in this locus, we integrated published proteomics data from another DO cohort (Chick et al., 2016) and one CC cohort, which shares the same founder strains with the DO (Keele et al., 2021). This strategy was based on the premise that evidence of consistent genetic effects

Figure 5. Genetic mapping of BA modulators

(A) Manhattan plot for QTL peaks of BA levels in the different biologically relevant compartments. The permutation-based p values for the QTL peaks of all BAs profiled in the liver, feces, and plasma were plotted along their genetic positions across different chromosomes. QTLs for BAs from CD-fed animals are indicated in triangles and dark colors, while the ones from HFD-fed mice are indicated in dots and light colors.

(B) QTL mapping of TUDCA plasma levels revealed a conserved QTL modulating TUDCA plasma levels on chromosome 8 from 80 to 110 Mb. The LOD score of the QTL is plotted in the y axis.

(C and E) The Manhattan plot for QTL peaks of BA ratios within each biological compartment (C), as well as BA ratios between different biological compartments (E). The permutation-based p values for the QTL peaks of all BA ratios were plotted along their genetic positions across different chromosomes. QTLs for BAs from CD-fed animals are indicated in triangles and dark colors, while the ones from HFD-fed mice are indicated in dots and light colors.

(D) QTL mapping of TUDCA to total BA ratio in plasma at T30 reveals a conserved QTL modulating TUDCA plasma levels on chromosome 8 from 80 to 110 Mb.

(F) QTL mapping of the ratio of secondary BAs in plasma T0 to liver identifies a QTL that modulates secondary BA levels on chromosome 1.

(G) Genetic position of *Cyp8b1* and *Abcb11* under the BA QTLs indicated in the legend and depicted with different colors in the plots.

(H) The Manhattan plot for QTL peaks of BA levels in different biological compartments together with QTL plots of all the metabolic phenotypes collected in an independent study (Williams et al., 2016).

(I) QTL mapping of plasma secondary (Sec.) BA levels and glucose levels at T0 in HFD-fed mice.

(J) QTL mapping of plasma secondary conjugated (Sec.conj.) BA levels and TDCA levels at T60, as well as RER max after wheel exercise in HFD-fed mice.

(K) Correlation heatmap between secondary conjugated BAs (plasma T60) and metabolic phenotypes in CD and HFD-fed mice. *$p < 0.05$ and **$p < 0.01$.

The upper dashed red lines in (A)–(J) indicate the threshold of genome-wide significance, and the lower dotted red lines indicate the suggestive threshold. A full list of the significant QTLs is provided in Table S6.

See also Figure S6 and Tables S1 and S7.

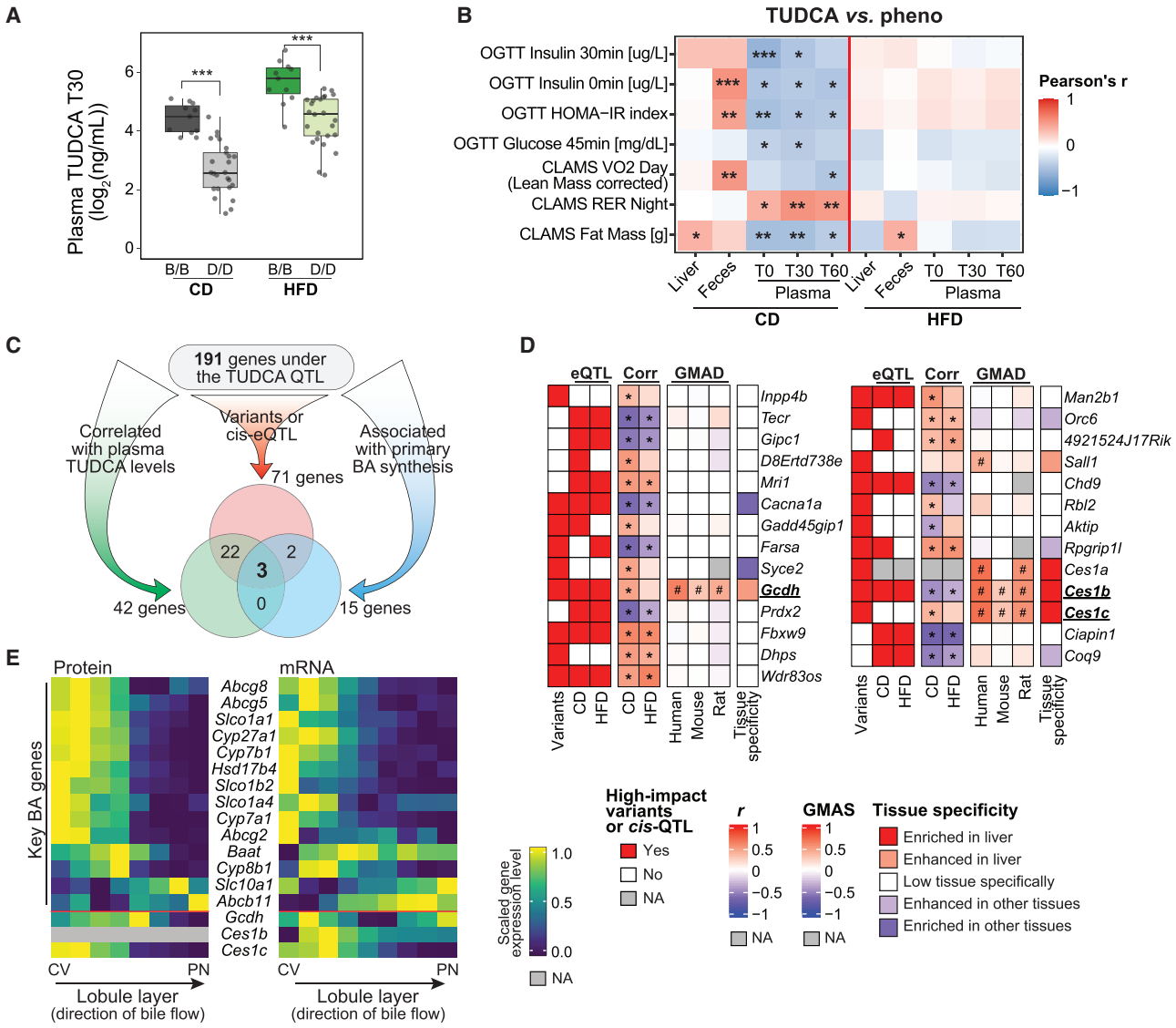

Figure 6. Genetic mapping of BA modulators and the identification of *Ces1c* as a potential regulator of plasma TUDCA levels

(A) The genetic effects of the TUDCA QTL on chromosome 8 on plasma TUDCA levels of the BXD animals at 30 min after a test meal. Plasma TUDCA concentrations (log_2 transformed data) were compared between strains inheriting the genetic allele from the reference C57BL/6J strain at the QTL (indicated as B/B) and those inheriting from the DBA/2J strain (indicated as D/D). ***$p < 0.001$ by two-tailed Student's t test.

(B) Heatmap presenting the correlations between the TUDCA levels across different biological compartments and phenotypic traits. *$p < 0.05$, **$p < 0.01$, and ***$p < 0.001$, for Pearson correlation coefficient.

(C) Systems genetics pipeline applied to filter for genes responsible for the plasma TUDCA QTL at T30 by integrating 3 major criteria, that is, (1) whether genes have high-impact genetic variants or *cis*-eQTLs in the liver, (2) whether their liver expression level correlates with plasma TUDCA levels at T30, and (3) whether they associate with the primary BA biosynthesis (KEGG 0120) pathway in GMAD (Li et al., 2019). The numbers of genes that fulfill each or several of these criteria are listed in the Venn diagram.

(D) Heatmap listing the genes under the plasma TUDCA QTL at T30 on chromosome 8 reveals the potential modulators of TUDCA. Only genes fulfilling at least 2 criteria were included in the heatmap. The first block of the heatmap represents whether the genes have high-impact variants or *cis*-eQTLs in liver transcriptome datasets of the BXDs. The second block (Corr) indicates the correlations between the liver expression of these genes and plasma TUDCA levels at T30 in CD or HFD. The third block shows the association between these genes and the primary BA biosynthesis pathway predicted by GMAD (Li et al., 2019) in human, mouse, and rat. The last block shows the enrichment of the expression of these genes in the liver, retrieved from the Human Protein Atlas (https://www.proteinatlas.org/) (Uhlén et al., 2015). *r*, Pearson correlation coefficient. GMAS, gene-module association score. Asterisk (*$p < 0.05$) and hash (#) indicate statistical significance in correlation and GMAD, respectively. The 3 selected candidates are in bold and underlined. Full list of the 191 genes under the TUDCA QTL on chromosome 8 is in Table S7.

(E) Zonation protein (left) or mRNA (right) profiles of key BA synthesis and transport genes, as well as candidate TUDCA modulators in the mouse liver. Protein or mRNA expression of each gene was scaled to 0–1.

See also Figure S6 and Tables S1, S8, and S9.

CellPress
OPEN ACCESS

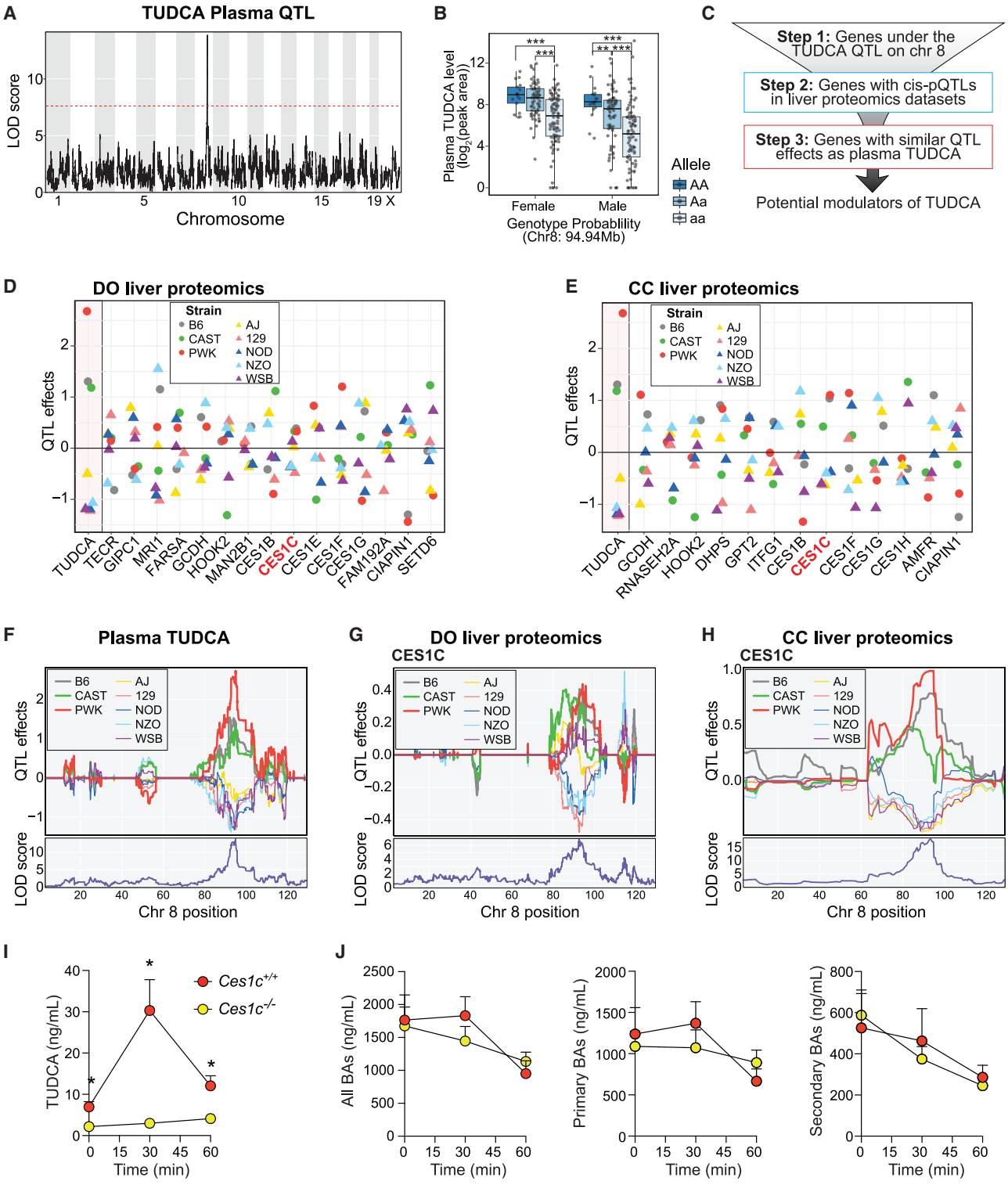

Figure 7. Validation of the causal link between *Ces1c* and TUDCA in DO or CC cohorts and *Ces1c*$^{-/-}$ mice

(A) QTL mapping results for fasting plasma TUDCA levels measured in a DO mouse cohort showing a significant peak at chromosome 8. The dashed red line indicates the threshold of genome-wide significance.

(B) The genetic effects of the TUDCA QTL on chromosome (Chr) 8 on fasting plasma TUDCA levels (log_2 data) of the DO animals. The genotype probability of the animals was calculated by considering the genetic allele of the C57BL/6J (B6), CAST/EiJ (CAST), and PWK/PhJ (PWK) strains as the reference allele (indicated as A) and the other allele as the alternative allele (indicated as a). **p < 0.01 and ***p < 0.001.

(legend continued on next page)

spanning these independent studies and our BXD study would lead to higher confidence in finding true causal genetic loci contributing to the regulation of TUDCA abundance.

To do so, we built an integrative systems genetics pipeline to prioritize the genes that are potential modulators of TUDCA levels (Figure 7C). Specifically, genes were first filtered if they had *cis*-pQTLs close to the TUDCA QTL in the liver proteomics datasets. Then, we estimated the founder strain haplotype effects on the protein levels of these genes and evaluated whether they were in concordance with the haplotype effects on the plasma TUDCA levels (Broman et al., 2019). C57BL/6J (B6), CAST/EiJ (CAST), and PWK/PhJ (PWK) founder haplotypes were associated with higher plasma TUDCA levels, while the other founder haplotypes with opposite effects (Figures 7D–7F). Proteins with similar haplotype effects as plasma TUDCA are most likely the key regulators of TUDCA (Figure 7C); in fact, the plasma TUDCA levels in the founder strains perfectly mirrored the estimated allele effects in the DO (Figures 7F, S7A, and S7B), highlighting the strong influence of genetics on TUDCA levels. For all proteins with a *cis*-pQTL in this locus in the DO or CC liver proteomics data, CES1C, but not CES1B or GCDH, showed similar patterns of haplotype effects as plasma TUDCA (Figures 7D–7H and S7C–S7F; Table S10), validating our analyses in the BXDs that *Ces1c* may be the key modulator for plasma TUDCA. The CES1C protein levels in the livers of the founder strains also resembled well the estimated allele effects in the DO and CC cohorts (Figures S7G–S7I).

Finally, to validate the results obtained from the *in silico* analyses and unequivocally establish the causal contribution of *Ces1c* in determining plasma TUDCA levels, we used a previously described *Ces1c* loss-of-function mouse model ($Ces1c^{-/-}$), where the exon 5 was deleted (Duysen et al., 2011). Plasma BA levels were measured in male $Ces1c^{-/-}$ and $Ces1c^{+/+}$ mice after a test meal bolus under the same experimental conditions as used for the BXD cohort (Figure 1A). In line with our analysis, TUDCA concentrations were significantly blunted upon loss of CES1C at all time points (Figure 7I), while the levels of the other BAs were unaffected or affected to a lesser extent (TCA at T30 only) by the loss of CES1C (Figures 7J and S8A–S8D). These data, together with the identification of CES1C as a novel modulator of TUDCA plasma levels, confirm that our systems genetics approach is a valuable tool to uncover novel modulators of BA homeostasis and metabolism.

DISCUSSION

Despite major advances in our understanding of the physiological roles of BAs, the full complexity of the genetic and environmental factors that control BA metabolism and signaling is only partially known. Several recent studies started to unveil genetic determinants of BAs using either human (Chen et al., 2020) or mouse (Kemis et al., 2019) cohorts. However, these studies did not explore the influence of dietary factors on BA homeostasis and the association of BAs with metabolic traits. To identify the determinants that control BA homeostasis in an unbiased fashion, we used a systems genetics approach that relies on a highly diverse cohort of BXD mouse lines and determined the BA abundance in the plasma, feces, and liver of about 360 animals fed either CD or HFD. We explored the BA diversity and established that it is modulated by both genetic and environmental factors, such as diet and nutritional status. Moreover, we demonstrated that the genetic background affects not only the BA amount and composition but also the response of BAs to feeding or HFD challenge. In general, HFD feeding increased primary BA abundance in all the analyzed biological compartments and decreased secondary BA levels, possibly explained by HFD-mediated imbalance in the gut microbial community. Furthermore, the abundance and composition of the BA amount in different biological compartments strongly correlated with metabolic performance, supporting the critical role of BAs in metabolic control. BAs in different compartments seemed to drive the association with specific metabolic traits in a highly regulated manner.

Despite the complexity of BA signaling, the combination of multi-omics data collected from the BXD mice allowed us to map hundreds of QTLs associated with BA abundance, including known regulators of BA synthesis and transport, such as *Cyp8b1* (Li-Hawkins et al., 2002), *Cyp7b1* (Li-Hawkins et al., 2000), and *Abcb11* (Gerloff et al., 1998), and to identify previously unknown BA modulators. In the current study, we focused our attention on the most significant QTL associated with plasma TUDCA levels. TUDCA is the major BA species in bear bile and is a well-known BA endowed with health-promoting effects (Cabrera et al., 2019; Häussinger and Kordes, 2017; Kusaczuk, 2019; Zangerolamo et al., 2021). Moreover, clinical trials have shown that TUDCA is effective in diseases ranging from amyotrophic lateral sclerosis (Elia et al., 2016), primary

(C) Systematic gene prioritization pipeline for plasma TUDCA regulators through the integration of liver proteomics data from independent DO (Chick et al., 2016) and CC (Keele et al., 2021) cohorts. The pipeline is composed of 3 steps. Step 1, keep only genes under the TUDCA QTL on chromosome (Chr) 8 for further filtering; step 2, extract genes with *cis*-pQTLs in the liver proteomics datasets; step 3, estimate the QTL haplotype effects on the protein levels of genes from step 2 and compare with those for plasma TUDCA.

(D and E) Dot plots showing the founder strain haplotype effects of the chromosome 8 QTL on plasma TUDCA and liver protein levels for candidate genes in step 2 of (C) in the DO (D) or CC (E) cohorts. Founder strains: 129S1/SvImJ (129), A/J (AJ), C57BL/6J (B6), NOD/ShiLtJ (NOD), NZO/HlLtJ (NZO), CAST/EiJ (CAST), PWK/PhJ (PWK), and WSB/EiJ (WSB). The founder strains were divided into two groups based on the direction of the haplotype effects on plasma TUDCA and labeled as circles and triangles, respectively. B6 and strains with the same allele as B6 at the Chr 8 TUDCA QTL showed higher plasma TUDCA and higher CES1C protein levels in the liver. Haplotype effects on protein levels of genes with *cis*-pQTL are available in Table S8.

(F–H) Founder strain QTL effects (upper) and QTL results (lower) of plasma TUDCA (F) and CES1C liver protein levels in DO (G) or CC (H) cohorts. For each plot, the x axis represents the genetic position on chromosome (Chr) 8. The y axis in the upper panel is the founder strain QTL effects, and the y axis in the lower panel is the LOD score for the QTL.

(I and J) Plasma TUDCA concentrations (I) and total (All), primary, and secondary BA concentrations (J) in $Ces1c^{+/+}$ (n = 9 mice) and $Ces1c^{-/-}$ (n = 11 mice) male mice (20-week-old, fed CD—following the timeline in Figure 1A) before and 30 or 60 min after oral administration of a test meal. *$p < 0.05$ versus $Ces1c^{+/+}$ by two-way ANOVA followed by Bonferroni post hoc test. Results are expressed as mean + SEM.

See also Figures S7 and S8 and Tables S1 and S10.

biliary cholangitis (Crosignani et al., 1996; Invernizzi et al., 1999; Larghi et al., 1997; Ma et al., 2016; Setchell et al., 1996), gallstones (Portincasa et al., 1996), and liver diseases (Crosignani et al., 1998; Pan et al., 2013). Furthermore, TUDCA was also shown to have clinical benefits in obese patients with insulin resistance (Kars et al., 2010), as well as in mice (Ozcan et al., 2006). Mechanistically, TUDCA acts as a chemical chaperone that alleviates endoplasmic reticulum stress (Cabrera et al., 2019; Ozcan et al., 2006) and by reducing the hydrophobicity of the BA pool (Cabrera et al., 2019).

We discovered *Ces1c* as a previously uncharacterized modulator gene of plasma TUDCA levels through a combination of *in silico* and *in vivo* experiments. The causal link between *Ces1c* and TUDCA that we established in the BXD mouse population is further validated using data obtained from independent DO and CC mouse cohorts, respectively (Chick et al., 2016; Keele et al., 2021; Kemis et al., 2019). The association between CES1C and plasma TUDCA levels was finally also ascertained by the striking reduction of TUDCA plasma levels in *Ces1c*$^{-/-}$ mice. Together these findings identify CES1C as an endogenous modulator of TUDCA levels. Further studies are warranted to mechanistically dissect how CES1C controls TUDCA levels and how these insights may translate into therapeutic applications for human metabolic diseases. Of note, CES1 is the predominant carboxylesterase expressed in the human liver. CES1 is involved in drug detoxification and metabolism of endogenous metabolites, including cholesterol and triglycerides (Redinbo et al., 2003). Interestingly, docking studies revealed that BAs can bind the catalytic site of CES1, with CDCA and TCA having the strongest binding activity (Kaddurah-Daouk et al., 2018). Further mechanistic studies will be required to gain further insight into this CES1-BA interaction.

The multi-omics data collected in this study will furthermore serve as a valuable resource for future studies to explore the genetic regulation of BAs and their relevance in health and disease. To facilitate the use of our data, we developed an interactive web interface at systems-genetics.org/BXD_BA. We expect that the web tool will support a community effort to fully leverage the rich information acquired in this multi-omics dataset, which ideally will support a better understanding of molecular mechanisms of BA homeostasis, as well as point to the pleiotropic roles of BAs in health and diseases.

In conclusion, we profiled postprandial BA abundance in physiologically relevant biological compartments from a large cohort of BXD mice and identified the genetic and environmental modulators of BAs. This approach led us to the identification and validation of CES1C as an uncharacterized modulator of plasma levels of TUDCA, a BA species with disease-modulating effects. We also provide the community with a mouse population resource to study BA homeostasis and its implications on metabolic health and disease.

Limitations of study

BA homeostasis is a complex biological process that relies on food-mediated enterohepatic recirculation, secretion into the systemic circulation, and excretion in the feces. Our study captured BA composition and abundance in postprandial liver and feces and monitored plasma changes in these parameters at 3 time points after administration of a controlled test meal. Although this experimental design provides a comprehensive picture of how genetics and diet regulate BA homeostasis in the different biological compartments, it does not reflect the dynamic complexity of this process. We had to choose one time point for the sacrifice of the animals, and we are aware that BA composition and amount in the liver would be different at another time point as BAs recycle between the liver and the intestine. Quantifying the BA pool size (total BA in the liver, gallbladder, and intestine) would also have been an important information, but this experimental design was incompatible with tissue biobanking for follow-up studies (e.g., comparison of hepatic metabolism in fasting versus feeding and analysis of the gut microbiome). Moreover, our study included only 36 BXD strains, and adding more strains would have allowed us to reach significance for more QTL signals and to narrow the QTL region. Still, 36 strains are sufficient to detect reliable genetic loci associated to BAs (Andreux et al., 2012; Wang et al., 2014). Finally, it is important to emphasize that BA composition is different in mice and humans, with the latter having a more hydrophobic BA pool and lacking the FXR antagonist TβMCA (Li and Dawson, 2019). However, studies in mouse GRPs, such as the BXDs, are essential to mimic the genetic diversity of humans and allow to standardize environmental factors and to get access to deep enterohepatic organs (Li and Auwerx, 2020).

STAR★METHODS

Detailed methods are provided in the online version of this paper and include the following:

- KEY RESOURCES TABLE
- RESOURCE AVAILABILITY
  - Lead Contact
  - Materials Availability
  - Data and Code Availability
- EXPERIMENTAL MODEL AND SUBJECT DETAILS
  - Clinical phenotyping tests
- METHOD DETAILS
  - BA quantification
- QUANTIFICATION AND STATISTICAL ANALYSIS
  - Microarray analysis
  - Heritability assessment
  - QTL mapping - BXD
  - Gene filtering
  - QTL mapping - DO
  - Single-cell RNA-seq analysis
  - Spatial transcriptomics analysis
- ADDITIONAL RESOURCES
  - Browsing dynamic multi-omics data in BXD-BA explorer

SUPPLEMENTAL INFORMATION

Supplemental information can be found online at https://doi.org/10.1016/j.cmet.2022.08.015.

ACKNOWLEDGMENTS

We thank Andréane Fouassier, Sabrina Bichet, Norman Moullan, Thibaud Clerc, Tony Teav, Rébecca Borreggine (Metabolomics Platform), the SV

animal facility (UDP), and the Schoonjans and Auwerx lab members for technical assistance and discussions. This work was supported by the École Polytechnique Fédérale de Lausanne (EPFL to K.S. and J.A.) and grants from the Kristian Gerhard Jebsen Foundation (to K.S. and J.A.), the European Research Council (ERC-AdG-787702 to J.A.), and the Swiss National Science Foundation (310030-189178 and CRSII5-180317 to K.S. and 31003A-179435 to J.A.). H.L. is the recipient of a doctoral scholarship from the China Scholarship Council (CSC). A.P. and L.A.V.-V. were supported by a postdoctoral fellowship from the AXA Research Fund. L.J.E.G. was supported by the European Union's Horizon 2020 research and innovation programme through the Marie Sklodowska-Curie Individual Fellowship "AmyloAge" (grant agreement no. 896042).

AUTHOR CONTRIBUTIONS

H.L., A.P., J.A., and K.S. conceived and designed the project. H.L., A.P., Q.H., L.A.V.-V., K.G., J. Imbach, and Y.S. performed animal experiments. M.K., H.G.-A., and J. Ivanisevic performed bile acid quantifications. H.L. and A.P. analyzed the data. A.B.-E., G.V.G.V.A., M.B.S., and L.J.E.G. created the web interface and contributed to the bioinformatic analysis of the data. A.B. analyzed the microarray data. X.L. prepared the data for submission to data repositories. E.G.W. provided expertise on the BXD GRP. H.L., A.P., J.A., and K.S. wrote the manuscript with input from all the authors.

DECLARATION OF INTERESTS

J.A. is a founder and/or consultant to MitoBridge/Astellas, Metro Biotech, Amazentis, and NOV Metapharma.

Received: December 15, 2021
Revised: June 22, 2022
Accepted: August 16, 2022
Published: September 12, 2022

REFERENCES

Aizarani, N., Saviano, A., Sagar, Mailly, L., Durand, S., Herman, J.S., Pessaux, P., Baumert, T.F., and Grün, D. (2019). A human liver cell atlas reveals heterogeneity and epithelial progenitors. Nature *572*, 199–204.

Andreux, P.A., Williams, E.G., Koutnikova, H., Houtkooper, R.H., Champy, M.F., Henry, H., Schoonjans, K., Williams, R.W., and Auwerx, J. (2012). Systems genetics of metabolism: the use of the BXD murine reference panel for multiscalar integration of traits. Cell *150*, 1287–1299.

Ben-Moshe, S., Shapira, Y., Moor, A.E., Manco, R., Veg, T., Bahar Halpern, K., and Itzkovitz, S. (2019). Spatial sorting enables comprehensive characterization of liver zonation. Nat. Metab. *1*, 899–911.

Bennett, B.J., Davis, R.C., Civelek, M., Orozco, L., Wu, J., Qi, H., Pan, C., Packard, R.R., Eskin, E., Yan, M., et al. (2015). Genetic architecture of atherosclerosis in mice: a systems genetics analysis of common inbred strains. PLoS Genet. *11*, e1005711.

Broman, K.W., Wu, H., Sen, S., and Churchill, G.A. (2003). R/qtl: QTL mapping in experimental crosses. Bioinformatics *19*, 889–890.

Broman, K.W., Gatti, D.M., Simecek, P., Furlotte, N.A., Prins, P., Sen, Ś., Yandell, B.S., and Churchill, G.A. (2019). R/qtl2: software for mapping quantitative trait loci with high-dimensional data and multiparent populations. Genetics *211*, 495–502.

Cabrera, D., Arab, J.P., and Arrese, M. (2019). UDCA, NorUDCA, and TUDCA in liver diseases: a review of their mechanisms of action and clinical applications. Handb. Exp. Pharmacol. *256*, 237–264.

Cani, P.D., Bibiloni, R., Knauf, C., Waget, A., Neyrinck, A.M., Delzenne, N.M., and Burcelin, R. (2008). Changes in gut microbiota control metabolic endotoxemia-induced inflammation in high-fat diet-induced obesity and diabetes in mice. Diabetes *57*, 1470–1481.

Chella Krishnan, K., Kurt, Z., Barrere-Cain, R., Sabir, S., Das, A., Floyd, R., Vergnes, L., Zhao, Y., Che, N., Charugundla, S., et al. (2018). Integration of multi-omics data from mouse diversity panel highlights mitochondrial dysfunction in non-alcoholic fatty liver disease. Cell Syst. *6*, 103–115.e7.

Chen, L., van den Munckhof, I.C.L., Schraa, K., Ter Horst, R., Koehorst, M., van Faassen, M., van der Ley, C., Doestzada, M., Zhernakova, D.V., Kurilshikov, A., et al. (2020). Genetic and microbial associations to plasma and fecal bile acids in obesity relate to plasma lipids and liver fat content. Cell Rep. *33*, 108212.

Chick, J.M., Munger, S.C., Simecek, P., Huttlin, E.L., Choi, K., Gatti, D.M., Raghupathy, N., Svenson, K.L., Churchill, G.A., and Gygi, S.P. (2016). Defining the consequences of genetic variation on a proteome-wide scale. Nature *534*, 500–505.

Cho, C.S., Xi, J., Si, Y., Park, S.R., Hsu, J.E., Kim, M., Jun, G., Kang, H.M., and Lee, J.H. (2021). Microscopic examination of spatial transcriptome using Seq-Scope. Cell *184*, 3559–3572.e22.

Crosignani, A., Battezzati, P.M., Setchell, K.D., Invernizzi, P., Covini, G., Zuin, M., and Podda, M. (1996). Tauroursodeoxycholic acid for treatment of primary biliary cirrhosis. A dose-response study. Dig. Dis. Sci. *41*, 809–815.

Crosignani, A., Budillon, G., Cimino, L., Del Vecchio Blanco, C., Loguercio, C., Ideo, G., Raimondo, G., Stabilini, R., and Podda, M. (1998). Tauroursodeoxycholic acid for the treatment of HCV-related chronic hepatitis: a multicenter placebo-controlled study. Hepatogastroenterology. *45*, 1624–1629.

David, L.A., Maurice, C.F., Carmody, R.N., Gootenberg, D.B., Button, J.E., Wolfe, B.E., Ling, A.V., Devlin, A.S., Varma, Y., Fischbach, M.A., et al. (2014). Diet rapidly and reproducibly alters the human gut microbiome. Nature *505*, 559–563.

Devkota, S., Wang, Y., Musch, M.W., Leone, V., Fehlner-Peach, H., Nadimpalli, A., Antonopoulos, D.A., Jabri, B., and Chang, E.B. (2012). Dietary-fat-induced taurocholic acid promotes pathobiont expansion and colitis in *Il10*$^{-/-}$ mice. Nature *487*, 104–108.

Duysen, E.G., Koentgen, F., Williams, G.R., Timperley, C.M., Schopfer, L.M., Cerasoli, D.M., and Lockridge, O. (2011). Production of ES1 plasma carboxylesterase knockout mice for toxicity studies. Chem. Res. Toxicol. *24*, 1891–1898.

Elia, A.E., Lalli, S., Monsurrò, M.R., Sagnelli, A., Taiello, A.C., Reggiori, B., La Bella, V., Tedeschi, G., and Albanese, A. (2016). Tauroursodeoxycholic acid in the treatment of patients with amyotrophic lateral sclerosis. Eur. J. Neurol. *23*, 45–52.

Gerloff, T., Stieger, B., Hagenbuch, B., Madon, J., Landmann, L., Roth, J., Hofmann, A.F., and Meier, P.J. (1998). The sister of P-glycoprotein represents the canalicular bile salt export pump of mammalian liver. J. Biol. Chem. *273*, 10046–10050.

Gieger, C., Geistlinger, L., Altmaier, E., Hrabé de Angelis, M., Kronenberg, F., Meitinger, T., Mewes, H.W., Wichmann, H.E., Weinberger, K.M., Adamski, J., et al. (2008). Genetics meets metabolomics: a genome-wide association study of metabolite profiles in human serum. PLoS Genet. *4*, e1000282.

Gu, Z., Gu, L., Eils, R., Schlesner, M., and Brors, B. (2014). circlize implements and enhances circular visualization in R. Bioinformatics *30*, 2811–2812.

Gu, Z., Eils, R., and Schlesner, M. (2016). Complex heatmaps reveal patterns and correlations in multidimensional genomic data. Bioinformatics *32*, 2847–2849.

Haeusler, R.A., Pratt-Hyatt, M., Welch, C.L., Klaassen, C.D., and Accili, D. (2012). Impaired generation of 12-hydroxylated bile acids links hepatic insulin signaling with dyslipidemia. Cell Metab. *15*, 65–74.

Haeusler, R.A., Astiarraga, B., Camastra, S., Accili, D., and Ferrannini, E. (2013). Human insulin resistance is associated with increased plasma levels of 12α-hydroxylated bile acids. Diabetes *62*, 4184–4191.

Halpern, K.B., Shenhav, R., Matcovitch-Natan, O., Toth, B., Lemze, D., Golan, M., Massasa, E.E., Baydatch, S., Landen, S., Moor, A.E., et al. (2017). Single-cell spatial reconstruction reveals global division of labour in the mammalian liver. Nature *542*, 352–356.

Hao, Y., Hao, S., Andersen-Nissen, E., Mauck, W.M., 3rd, Zheng, S., Butler, A., Lee, M.J., Wilk, A.J., Darby, C., Zager, M., et al. (2021). Integrated analysis of multimodal single-cell data. Cell *184*, 3573–3587.e29.

Harach, T., Pols, T.W., Nomura, M., Maida, A., Watanabe, M., Auwerx, J., and Schoonjans, K. (2012). TGR5 potentiates GLP-1 secretion in response to anionic exchange resins. Sci. Rep. *2*, 430.

Häussinger, D., and Kordes, C. (2017). Mechanisms of tauroursodeoxycholate-mediated hepatoprotection. Dig. Dis. *35*, 224–231.

Hildebrandt, M.A., Hoffmann, C., Sherrill-Mix, S.A., Keilbaugh, S.A., Hamady, M., Chen, Y.Y., Knight, R., Ahima, R.S., Bushman, F., and Wu, G.D. (2009). High-fat diet determines the composition of the murine gut microbiome independently of obesity. Gastroenterology *137*, 1716–1724.e1–2.

Hui, S.T., Kurt, Z., Tuominen, I., Norheim, F., Davis, R.C., Pan, C., Dirks, D.L., Magyar, C.E., French, S.W., Chella Krishnan, K., et al. (2018). The genetic architecture of diet-induced hepatic fibrosis in mice. Hepatology *68*, 2182–2196.

Invernizzi, P., Setchell, K.D., Crosignani, A., Battezzati, P.M., Larghi, A., O'Connell, N.C., and Podda, M. (1999). Differences in the metabolism and disposition of ursodeoxycholic acid and of its taurine-conjugated species in patients with primary biliary cirrhosis. Hepatology *29*, 320–327.

Irizarry, R.A., Hobbs, B., Collin, F., Beazer-Barclay, Y.D., Antonellis, K.J., Scherf, U., and Speed, T.P. (2003). Exploration, normalization, and summaries of high density oligonucleotide array probe level data. Biostatistics *4*, 249–264.

Jha, P., McDevitt, M.T., Gupta, R., Quiros, P.M., Williams, E.G., Gariani, K., Sleiman, M.B., Diserens, L., Jochem, A., Ulbrich, A., et al. (2018a). Systems analyses reveal physiological roles and genetic regulators of liver lipid species. Cell Syst. *6*, 722–733.e6.

Jha, P., McDevitt, M.T., Halilbasic, E., Williams, E.G., Quiros, P.M., Gariani, K., Sleiman, M.B., Gupta, R., Ulbrich, A., Jochem, A., et al. (2018b). Genetic regulation of plasma lipid species and their association with metabolic phenotypes. Cell Syst. *6*, 709–721.e6.

Kaddurah-Daouk, R., Hankemeier, T., Scholl, E.H., Baillie, R., Harms, A., Stage, C., Dalhoff, K.P., Jürgens, G., Taboureau, O., Nzabonimpa, G.S., et al. (2018). Pharmacometabolomics informs about pharmacokinetic profile of methylphenidate. CPT Pharmacometrics Syst. Pharmacol. *7*, 525–533.

Kars, M., Yang, L., Gregor, M.F., Mohammed, B.S., Pietka, T.A., Finck, B.N., Patterson, B.W., Horton, J.D., Mittendorfer, B., Hotamisligil, G.S., and Klein, S. (2010). Tauroursodeoxycholic acid may improve liver and muscle but not adipose tissue insulin sensitivity in obese men and women. Diabetes *59*, 1899–1905.

Keele, G.R., Zhang, T., Pham, D.T., Vincent, M., Bell, T.A., Hock, P., Shaw, G.D., Paulo, J.A., Munger, S.C., de Villena, P.-M., et al. (2021). Regulation of protein abundance in genetically diverse mouse populations. Cell Genomics *1*, 100003.

Kemis, J.H., Linke, V., Barrett, K.L., Boehm, F.J., Traeger, L.L., Keller, M.P., Rabaglia, M.E., Schueler, K.L., Stapleton, D.S., Gatti, D.M., et al. (2019). Genetic determinants of gut microbiota composition and bile acid profiles in mice. PLoS Genet. *15*, e1008073.

Kuipers, F., Bloks, V.W., and Groen, A.K. (2014). Beyond intestinal soap—bile acids in metabolic control. Nat. Rev. Endocrinol. *10*, 488–498.

Kusaczuk, M. (2019). Tauroursodeoxycholate-bile acid with chaperoning activity: molecular and cellular effects and therapeutic perspectives. Cells *8*, 1471.

Larghi, A., Crosignani, A., Battezzati, P.M., De Valle, G., Allocca, M., Invernizzi, P., Zuin, M., and Podda, M. (1997). Ursodeoxycholic and tauro-ursodeoxycholic acids for the treatment of primary biliary cirrhosis: a pilot crossover study. Aliment. Pharmacol. Ther. *11*, 409–414.

Li, H., and Auwerx, J. (2020). Mouse systems genetics as a prelude to precision medicine. Trends Genet. *36*, 259–272.

Li, J., and Dawson, P.A. (2019). Animal models to study bile acid metabolism. Biochim. Biophys. Acta Mol. Basis Dis. *1865*, 895–911.

Li, H., Wang, X., Rukina, D., Huang, Q., Lin, T., Sorrentino, V., Zhang, H., Bou Sleiman, M., Arends, D., McDaid, A., et al. (2018). An integrated systems genetics and omics toolkit to probe gene function. Cell Syst. *6*, 90–102.e4.

Li, H., Rukina, D., David, F.P.A., Li, T.Y., Oh, C.M., Gao, A.W., Katsyuba, E., Bou Sleiman, M., Komljenovic, A., Huang, Q., et al. (2019). Identifying gene function and module connections by the integration of multispecies expression compendia. Genome Res. *29*, 2034–2045.

Li-Hawkins, J., Lund, E.G., Turley, S.D., and Russell, D.W. (2000). Disruption of the oxysterol 7α-hydroxylase gene in mice. J. Biol. Chem. *275*, 16536–16542.

Li-Hawkins, J., Gåfvels, M., Olin, M., Lund, E.G., Andersson, U., Schuster, G., Björkhem, I., Russell, D.W., and Eggertsen, G. (2002). Cholic acid mediates negative feedback regulation of bile acid synthesis in mice. J. Clin. Invest. *110*, 1191–1200.

Linke, V., Overmyer, K.A., Miller, I.J., Brademan, D.R., Hutchins, P.D., Trujillo, E.A., Reddy, T.R., Russell, J.D., Cushing, E.M., Schueler, K.L., et al. (2020). A large-scale genome-lipid association map guides lipid identification. Nat. Metab. *2*, 1149–1162.

Ma, H., Zeng, M., Han, Y., Yan, H., Tang, H., Sheng, J., Hu, H., Cheng, L., Xie, Q., Zhu, Y., et al. (2016). A multicenter, randomized, double-blind trial comparing the efficacy and safety of TUDCA and UDCA in Chinese patients with primary biliary cholangitis. Medicine (Baltimore) *95*, e5391.

Marion, S., Desharnais, L., Studer, N., Dong, Y., Notter, M.D., Poudel, S., Menin, L., Janowczyk, A., Hettich, R.L., Hapfelmeier, S., and Bernier-Latmani, R. (2020). Biogeography of microbial bile acid transformations along the murine gut. J. Lipid Res. *61*, 1450–1463.

Nadeau, J.H., and Auwerx, J. (2019). The virtuous cycle of human genetics and mouse models in drug discovery. Nat. Rev. Drug Discov. *18*, 255–272.

Norheim, F., Hasin-Brumshtein, Y., Vergnes, L., Chella Krishnan, K., Pan, C., Seldin, M.M., Hui, S.T., Mehrabian, M., Zhou, Z., Gupta, S., et al. (2019). Gene-by-sex interactions in mitochondrial functions and cardio-metabolic traits. Cell Metab. *29*, 932–949.e4.

Ozcan, U., Yilmaz, E., Ozcan, L., Furuhashi, M., Vaillancourt, E., Smith, R.O., Görgün, C.Z., and Hotamisligil, G.S. (2006). Chemical chaperones reduce ER stress and restore glucose homeostasis in a mouse model of type 2 diabetes. Science *313*, 1137–1140.

Pan, X.L., Zhao, L., Li, L., Li, A.H., Ye, J., Yang, L., Xu, K.S., and Hou, X.H. (2013). Efficacy and safety of tauroursodeoxycholic acid in the treatment of liver cirrhosis: a double-blind randomized controlled trial. J. Huazhong Univ. Sci. Technolog. Med. Sci. *33*, 189–194.

Parker, B.L., Calkin, A.C., Seldin, M.M., Keating, M.F., Tarling, E.J., Yang, P., Moody, S.C., Liu, Y., Zerenturk, E.J., Needham, E.J., et al. (2019). An integrative systems genetic analysis of mammalian lipid metabolism. Nature *567*, 187–193.

Perino, A., and Schoonjans, K. (2022). Metabolic messengers: bile acids. Nat. Metab. *4*, 416–423.

Perino, A., Demagny, H., Velazquez-Villegas, L.A., and Schoonjans, K. (2020). Molecular physiology of bile acid signaling in health, disease and aging. Physiol. Rev. *101*, 683–731.

Perino, A., Velázquez-Villegas, L.A., Bresciani, N., Sun, Y., Huang, Q., Fénelon, V.S., Castellanos-Jankiewicz, A., Zizzari, P., Bruschetta, G., Jin, S., et al. (2021). Central anorexigenic actions of bile acids are mediated by TGR5. Nat. Metab. *3*, 595–603.

Portincasa, P., DiCiaula, A., Palmieri, V., Velardi, A., Van Berge-Henegouwen, G.P., and Palasciano, G. (1996). Tauroursodeoxycholic acid, ursodeoxycholic acid and gallbladder motility in gallstone patients and healthy subjects. Ital. J. Gastroenterol. *28*, 111–113.

Qin, Y., Wang, Y., Liu, O., Jia, L., Fang, W., Du, J., and Wei, Y. (2017). Tauroursodeoxycholic acid attenuates angiotensin II induced abdominal aortic aneurysm formation in apolipoprotein E-deficient mice by inhibiting endoplasmic reticulum stress. Eur. J. Vasc. Endovasc. Surg. *53*, 337–345.

Redinbo, M.R., Bencharit, S., and Potter, P.M. (2003). Human carboxylesterase 1: from drug metabolism to drug discovery. Biochem. Soc. Trans. *31*, 620–624.

Rodrigues, C.M., Sola, S., Nan, Z., Castro, R.E., Ribeiro, P.S., Low, W.C., and Steer, C.J. (2003). Tauroursodeoxycholic acid reduces apoptosis and protects against neurological injury after acute hemorrhagic stroke in rats. Proc. Natl. Acad. Sci. USA *100*, 6087–6092.

Russell, D.W. (2003). The enzymes, regulation, and genetics of bile acid synthesis. Annu. Rev. Biochem. *72*, 137–174.

Sasaki, T., Watanabe, Y., Kuboyama, A., Oikawa, A., Shimizu, M., Yamauchi, Y., and Sato, R. (2021). Muscle-specific TGR5 overexpression improves glucose clearance in glucose-intolerant mice. J. Biol. Chem. *296*, 100131.

Sayin, S.I., Wahlström, A., Felin, J., Jäntti, S., Marschall, H.U., Bamberg, K., Angelin, B., Hyötyläinen, T., Orešič, M., and Bäckhed, F. (2013). Gut microbiota regulates bile acid metabolism by reducing the levels of tauro-beta-muricholic acid, a naturally occurring FXR antagonist. Cell Metab. *17*, 225–235.

Schaap, F.G., Trauner, M., and Jansen, P.L. (2014). Bile acid receptors as targets for drug development. Nat. Rev. Gastroenterol. Hepatol. *11*, 55–67.

Selwyn, F.P., Csanaky, I.L., Zhang, Y., and Klaassen, C.D. (2015). Importance of large intestine in regulating bile acids and glucagon-like peptide-1 in germfree mice. Drug Metab. Dispos. *43*, 1544–1556.

Setchell, K.D., Rodrigues, C.M., Podda, M., and Crosignani, A. (1996). Metabolism of orally administered tauroursodeoxycholic acid in patients with primary biliary cirrhosis. Gut *38*, 439–446.

Shin, S.Y., Fauman, E.B., Petersen, A.K., Krumsiek, J., Santos, R., Huang, J., Arnold, M., Erte, I., Forgetta, V., Yang, T.P., et al. (2014). An atlas of genetic influences on human blood metabolites. Nat. Genet. *46*, 543–550.

Smallwood, T.L., Gatti, D.M., Quizon, P., Weinstock, G.M., Jung, K.C., Zhao, L., Hua, K., Pomp, D., and Bennett, B.J. (2014). High-resolution genetic mapping in the diversity outbred mouse population identifies Apobec1 as a candidate gene for atherosclerosis. G3 (Bethesda) *4*, 2353–2363.

Sonnenburg, J.L., and Bäckhed, F. (2016). Diet-microbiota interactions as moderators of human metabolism. Nature *535*, 56–64.

Sorrentino, G., Perino, A., Yildiz, E., El Alam, G., Bou Sleiman, M., Gioiello, A., Pellicciari, R., and Schoonjans, K. (2020). Bile acids signal via TGR5 to activate intestinal stem cells and epithelial regeneration. Gastroenterology *159*, 956–968.e8.

Thomas, C., Gioiello, A., Noriega, L., Strehle, A., Oury, J., Rizzo, G., Macchiarulo, A., Yamamoto, H., Mataki, C., Pruzanski, M., et al. (2009). TGR5-mediated bile acid sensing controls glucose homeostasis. Cell Metab. *10*, 167–177.

Uhlén, M., Fagerberg, L., Hallström, B.M., Lindskog, C., Oksvold, P., Mardinoglu, A., Sivertsson, Å., Kampf, C., Sjöstedt, E., Asplund, A., et al. (2015). Proteomics. Tissue-based map of the human proteome. Science *347*, 1260419.

Velazquez-Villegas, L.A., Perino, A., Lemos, V., Zietak, M., Nomura, M., Pols, T.W.H., and Schoonjans, K. (2018). TGR5 signalling promotes mitochondrial fission and beige remodelling of white adipose tissue. Nat. Commun. *9*, 245.

Visscher, P.M., Wray, N.R., Zhang, Q., Sklar, P., McCarthy, M.I., Brown, M.A., and Yang, J. (2017). 10 years of GWAS discovery: biology, function, and translation. Am. J. Hum. Genet. *101*, 5–22.

Wahlström, A., Sayin, S.I., Marschall, H.U., and Bäckhed, F. (2016). Intestinal crosstalk between bile acids and microbiota and its impact on host metabolism. Cell Metab. *24*, 41–50.

Wang, L., Jiao, Y., Cao, Y., Liu, G., Wang, Y., and Gu, W. (2014). Limitation of number of strains and persistence of false positive loci in QTL mapping using recombinant inbred strains. PLoS One *9*, e102307.

Watanabe, M., Houten, S.M., Mataki, C., Christoffolete, M.A., Kim, B.W., Sato, H., Messaddeq, N., Harney, J.W., Ezaki, O., Kodama, T., et al. (2006). Bile acids induce energy expenditure by promoting intracellular thyroid hormone activation. Nature *439*, 484–489.

Wickham, H. (2016). ggplot2: Elegant Graphics for Data Analysis (Springer-Verlag).

Williams, E.G., Wu, Y., Jha, P., Dubuis, S., Blattmann, P., Argmann, C.A., Houten, S.M., Amariuta, T., Wolski, W., Zamboni, N., et al. (2016). Systems proteomics of liver mitochondria function. Science *352*, aad0189.

Xia, S.W., Wang, Z.M., Sun, S.M., Su, Y., Li, Z.H., Shao, J.J., Tan, S.Z., Chen, A.P., Wang, S.J., Zhang, Z.L., et al. (2020). Endoplasmic reticulum stress and protein degradation in chronic liver disease. Pharmacol. Res. *161*, 105218.

Zangerolamo, L., Vettorazzi, J.F., Rosa, L.R.O., Carneiro, E.M., and Barbosa, H.C.L. (2021). The bile acid TUDCA and neurodegenerative disorders: an overview. Life Sci. *272*, 119252.

STAR★METHODS

KEY RESOURCES TABLE

REAGENT or RESOURCE	SOURCE	IDENTIFIER
Critical commercial assays		
Affymetrix mouse Clariom S	Affymetrix	Cat#902931
Deposited data		
BXD bile acid data from this study	This study	https://mpdpreview.jax.org/projects/Schoonjans1
BXD phenotype data from this study	This study	https://mpdpreview.jax.org/projects/Schoonjans1
BXD liver transcriptomics data from this study	This study	GEO: GSE188764
Resource website for the described data and analysis tools	This study	https://www.systems-genetics.org/BXD_BA
Data S1 - Source Data	This study	N/A
Human liver scRNA-seq data	Aizarani et al., 2019	GEO: GSE124395
Mouse liver scRNA-seq data	Halpern et al., 2017	GEO: GSE84498
Mouse liver proteomics data	Ben-Moshe et al., 2019	https://static-content.springer.com/esm/art%3A10.1038%2Fs42255-019-0109-9/MediaObjects/42255_2019_109_MOESM6_ESM.xlsx
Mouse liver spatial transcriptomics data	Cho et al., 2021	https://www.sciencedirect.com/science/article/pii/S0092867421006279#mmc2
DO plasma bile acid data	Kemis et al., 2019	https://chorusproject.org/pages/dashboard.html#/search/bile/projects/1568/experiments/3380/files
Founder strain plasma bile acid data	Kemis et al., 2019	https://chorusproject.org/pages/dashboard.html#/search/bile/projects/1568/experiments/3382/files
DO liver proteomics data	Chick et al., 2016	https://churchilllab.jax.org/qtlviewer/svenson/DOHFD
CC liver proteomics data	Keele et al., 2021	https://churchilllab.jax.org/qtlviewer/CC/Ferris
CC founder proteomics data	Chick et al., 2016	https://static-content.springer.com/esm/art%3A10.1038%2Fnature18270/MediaObjects/41586_2016_BFnature18270_MOESM75_ESM.zip
Tissue specific gene expression data	Uhlén et al., 2015	https://www.proteinatlas.org/humanproteome/tissue/liver
Gene-module association results	Li et al., 2019	https://www.systems-genetics.org/genebridge
Experimental models: Organisms/strains		
Mouse: BXD strains	University of Tennessee Health Science Center	N/A
Mouse: B6.Cg-*Ces1c*$^{tm1.1Loc}$/J (*Ces1c*$^{+/+}$ and *Ces1c*$^{-/-}$)	The Jackson Laboratory	JAX: 014096
Software and algorithms		
R	The R Foundation	https://www.r-project.org/
R/qtl	Broman et al., 2003	http://www.rqtl.org/
R/qtl2	Broman et al., 2019	https://kbroman.org/qtl2/
R/Seurat	Hao et al., 2021	https://cloud.r-project.org/%E2%80%8Bpackage=Seurat
R/ComplexHeatmap	Gu et al., 2016	https://bioconductor.org/packages/release/bioc/html/ComplexHeatmap.html
R/ggplot2	Wickham, 2016	https://ggplot2.tidyverse.org/

(*Continued on next page*)

Continued

REAGENT or RESOURCE	SOURCE	IDENTIFIER
R/circlize	Gu et al., 2014	https://cran.r-project.org/web/packages/circlize/
Prism GraphPad	GraphPad Software	Prism 9
Other		
Chow diet	Envigo	2018
High fat diet	Envigo	TD.06414
Ensure Plus	Ensure	https://www.puravita.ch/fr_ch/ensure-plus-liquide-fraise-24-200-ml
Liquid chromatography - high-resolution mass spectrometry	ThermoFisher Scientific	N/A

RESOURCE AVAILABILITY

Lead Contact

Further information and requests for resources and reagents should be directed to and will be fulfilled by the Lead Contact, Kristina Schoonjans (kristina.schoonjans@epfl.ch).

Materials Availability

This study did not generate new unique reagents.

Data and Code Availability

- The liver transcriptomics data have been uploaded to the Gene Expression Omnibus (GEO) with the accession ID GEO: GSE188764. The bile acid and phenotypic data have been deposited to the Mouse Phenotype Database (https://phenome.jax.org/) under the project "Schoonjans1" and GeneNetwork (http://www.genenetwork.org), which are open-access repositories that provide analytical tool suitable for the entire scientific community. The systems genetics results described in this manuscript are also available at the interactive webtool (systems-genetics.org/BXD_BA). The values used to create the graphs in the paper are provided as Data S1 - Source Data.
- This paper does not report original code.
- Any additional information required to reanalyze the data reported in this paper is available from the Lead Contact upon request.

EXPERIMENTAL MODEL AND SUBJECT DETAILS

Clinical phenotyping tests

The BXD strains were acquired from the University of Tennessee Health Science Center (Memphis, TN, USA) and bred at the Center of PhenoGenomics (SV-CPG) at Ecole Polytechnique Fédérale de Lausanne (EPFL) for over 20 generations. Approximately 360 male mice from 34 BXD strains and 2 parental strains were included in this study. 8-week-old male mice were fed either the Teklad Global 18% Protein Rodent Diet 2018 chow diet (24% kCal of protein, 18% kCal of fat, 58% kCal of carbohydrate – Envigo, Indianapolis, USA) or the Teklad Custom Diet TD.06414 high-fat diet (18.3% kCal of protein, 60.3% kCal of fat, 21.4% kCal of carbohydrate – Envigo, Indianapolis, USA), which mimics current energy-dense diets humans are consuming. All mice were housed under 12 h light/dark cycle (lights on at 7am), with a temperature of 22°C ± 1°C. A summary of the phenotyping pipeline is included in Figure 1A. Gross health status inspection of all mice was performed daily by experienced animal caretakers. Body weight was recorded before each phenotyping.

BA kinetics

At 20 weeks of age, the mice were fasted overday (9am-7pm) to allow bile accumulation in the gallbladder, then gavaged with Ensure Plus (10ml/Kg) (Harach et al., 2012) at 7pm to mimic a standardized postprandial state. Glycemia values and plasma were collected at 0, 30, and 60 min after the gavage. Body weight was recorded before and after the overday fasting.

Feces collection

Mice were single caged and feces were collected over a period of 24h at 24 weeks of age. To avoid coprophagy, the animals were placed on a grid, with ad libitum access to food and water. Feces were collected at the end of the experiment and frozen for further analysis.

Animal sacrifice

To avoid multiple sacrifices at night, the light/dark cycle of the mice was inverted two weeks before the sacrifice to ensure their adaptation. At 29 weeks of age, mice were fasted overnight (their day) and refed with their respective diet for 4 hours before sacrifice. Liver samples were collected and the gallbladder was discarded. The samples were immediately frozen in liquid nitrogen and stored at –80°C until analysis.

Ces1c$^{-/-}$ *mice*

Ces1c knock-out mice (*Ces1c*$^{-/-}$) were purchased from Jackson Laboratory (B6.Cg-*Ces1c*$^{tm1.1Loc}$/J, JAX stock #014096 – MGI Direct Data Submission MGI: J:168821) (Duysen et al., 2011). *Ces1c*$^{-/-}$ mice, lacking exon 5 of the *Ces1c* gene and abolishing gene function, were donated to JAX by Dr. Oksana Lockridge (Eppley Institute, University of Nebraska Medical Center). *Ces1c*$^{-/-}$ mice on a C57BL/6J background were bred in house with C57BL/6J mice (Charles River). 20-week-old *Ces1c*$^{-/-}$ and *Ces1c*$^{+/+}$ male mice fed CD (Teklad Global 18% Protein Rodent Diet 2018) were subjected to a BA kinetic experiment, following the method described above.

Ethical approval of animal studies

All animal experiments were approved by the Swiss cantonal veterinary authorities of Vaud under the licenses 2257.2 and 3699.

METHOD DETAILS

BA quantification

BAs were quantified using the stable isotope dilution mass spectrometry assay at the Metabolomics Platform of the University of Lausanne. Standard solutions for calibration, Quality Controls (QCs), and samples were prepared as described previously (Sorrentino et al., 2020). Briefly, calibrators were prepared by serial dilutions with stripped serum (C0-C7). Internal standard (IS) mixture contained 13 deuterium-labeled (d4-d5) BAs (listed in Table S1).

Sample preparation

The frozen liver and lyophilized fecal samples were ground with liquid nitrogen using mortar and pestle, pre-weighed in the lysis tubes, and homogenized in tissue homogenizer (Precellys Cryolys, Bertin Technologies SAS) by the addition of MeOH:H_2O (2:1) with 0.1% FA (1500 μL) and ceramic beads (for 2 × 20 seconds at 10,000 rpm). Homogenized extracts were centrifuged for 15 minutes at 21,000 g at 4°C, and the aliquots (50 μL) of supernatants were pre-mixed with 100 μL of the ice-cold IS mixture (in 100% MeOH), and 600 μL of H_2O with 0.2% formic acid, and loaded onto solid-phase extraction (SPE) plates for further processing as previously described (Sorrentino et al., 2020). Plasma aliquots (25 μL) were prepared in the same way (with the addition of the IS mixture) and processed using SPE for the phospholipid removal and BA pre-concentration.

Liquid chromatography - high-resolution mass spectrometry (LC-HRMS) analysis

BA quantification was performed on a LC-HRMS system (Vanquish Horizon UHPLC coupled with Q-Exactive Focus mass spectrometer interfaced with a HESI source, ThermoFisher Scientific) operating in negative ionization mode. Chromatographic separation was carried out using an Acquity UPLC HSS T3 1.8 μm 2.1 x 100 mm column. The mobile phase was composed of A = 5 mM Ammonium Acetate and 0.1% formic acid in H_2O and B = 0.1% formic acid in ACN. Gradient elution was set as described in the table below. The flow rate was 350 μL/min, the column temperature 30°C, and the injection volume 20 μL. Mass spectrometry parameters were set as follows: full scan in narrow mass range m/z 370-522, mass resolving power = 70,000 FWHM and AGC target = 5e5. Data were processed as described previously (Sorrentino et al., 2020). BA concentrations were reported to the tissue fresh (i.e. frozen) weight and feces dry weight.

Elution gradient for chromatographic separation of BAs

t min	A %	B %
0	70	30
6	70	30
6.1	65	35
9	65	35
9.1	58	42
16.5	55	45
17	25	75
21	25	75
21.1	0	100
26	0	100
26.1	70	30
30	70	30

QUANTIFICATION AND STATISTICAL ANALYSIS

Microarray analysis

About 100 mg of fresh frozen liver tissue for each mouse was suspended in TRIzol (Thermo Fisher Scientific) and then homogenized using TissueLyser II (QIAGEN). mRNA was then extracted using chloroform and precipitated using isopropanol. The concentration of mRNA was measured using NanoDrop (Thermo Fisher Scientific). mRNA samples for each strain fed with the same diet were pooled equally and then cleaned up using RNEasy (QIAGEN). 35 of the 36 pooled samples had a RNA integrity number (RIN) over 8.0 and the

other one sample had a RIN of 7.9, indicating that they were of high quality and could be used for subsequent microarray analysis. Microarrays were run using the Affymetrix mouse Clariom S Array at the Molecular Resource Center of Excellence in The University of Tennessee Health Science Center. Data were normalized using the RMA method (Irizarry et al., 2003), then analyzed in house using custom scripts in R.

Heritability assessment

Heritability estimates the extent of genetic contributions to trait variations. Heritability of the BA levels was calculated using either one-way (CD or HFD) or two-way (mixed) analysis of variance.

QTL mapping - BXD

BA measures and liver transcript levels were winsorized to account for possibly spurious outliers, and Box-Cox transformation was applied to transform the data into normal distribution. R/qtl package was used to map the QTL of the traits (Broman et al., 2003). Significance of the QTLs were determined through 10,000 permutation tests.

Gene filtering

Genes under the plasma TUDCA QTL at T30 on chromosome 8 were filtered based on several criteria, including: 1) whether the gene had high-impact genetic variants (including missense, nonsense, splice site, frameshift mutations, copy number variations) or *cis*-eQTLs in liver transcriptome in the BXDs; 2) whether expression levels of the gene correlated with plasma TUDCA levels at 30 minutes after gavage in CD or HFD; 3) whether the gene associated with primary BA biosynthesis pathway module (KEGG 0120) using liver datasets predicted by gene-module association determination (GMAD), a systems genetics approach based on large-scale expression datasets (https://systems-genetics.org/) (Li et al., 2019). In the GMAD analysis, 51 human, 63 mouse, and 18 rat liver transcriptomics datasets with over 80 samples were used to infer the associations between pathway modules and genes. In addition, since TUDCA is a primary BA synthesized in the liver in mice, we checked the specific expression of these genes in the liver. The tissue specificity gene expression data was downloaded from the Human Protein Atlas (https://proteinatlas.org/humanproteome/tissue/liver) (Uhlén et al., 2015) on 2019.12.18.

QTL mapping - DO

Plasma BA measurements from the DO animals and the founder strains were downloaded from Chorus (https://chorusproject.org/pages/index.html) with the project ID 1568, and $\log_2$ transformed for further analyses (Kemis et al., 2019). R/qtl2 package was used for QTL mapping (Broman et al., 2019). To account for the genetic similarities between animals, the kinship matrix was determined using the leave-one-chromosome-out (LOCO) method. Genome scan of the BAs was performed with the sex, cohort, and days on diet as additive covariates, and with the kinship as random effects. The founder strain haplotype effect was estimated using the Best Linear Unbiased Predictors (BLUPs) model in the R/qtl2 package (Broman et al., 2019). Liver pQTL data from the CC (Keele et al., 2021) and DO (Chick et al., 2016) mouse cohorts were retrieved from https://churchilllab.jax.org/qtlviewer/CC/Ferris and https://churchilllab.jax.org/qtlviewer/svenson/DOHFD, respectively, on October 5, 2020.

Single-cell RNA-seq analysis

Spatial zonation transcriptomics and proteomics profiles of mouse liver genes were obtained from (Ben-Moshe et al., 2019; Halpern et al., 2017). Human and mouse liver single-cell RNA-seq data were retrieved from (Aizarani et al., 2019; Halpern et al., 2017), and analyzed using R/Seurat package (Hao et al., 2021).

Spatial transcriptomics analysis

The spatial cluster-specific expression patterns of genes in hepatocytes were obtained from (Cho et al., 2021). Briefly, Seq-Scope, a barcoding technology that profiles spatial transcriptome at a sub-micrometer resolution, was performed on the livers of normal and $Tsc1^{\Delta hep}$/$Depdc5^{\Delta hep}$ (TD) mice. Pericentral (PC) and periportal (PP) hepatocytes were identified using cell type mapping analysis. The specific expression patterns of genes in PC hepatocytes were identified through the FindAllMarkers function in the R/Seurat package (Hao et al., 2021).

ADDITIONAL RESOURCES

Browsing dynamic multi-omics data in BXD-BA explorer

In this study, we laid a multi-omics data foundation to study the genetic and environmental regulators of BA homeostasis. We consider that our dataset, constituted by genomic, transcriptomic, and BA measurements of 36 BXD strains (~360 animals) fed CD or HFD can be a valuable resource for any future investigation in the field. To support data mining and result exploration we released an interactive web-tool accessible at http://systems-genetics.org/BXD_BA. This resource offers analysis and visualisation options for raw data exploration and for reproduction of the results presented above. A guide including an overview and some examples of data exploration is available as supplemental information.

Cell Metabolism, Volume *34*

Supplemental information

Integrative systems analysis identifies genetic and dietary modulators of bile acid homeostasis

Hao Li, Alessia Perino, Qingyao Huang, Giacomo V.G. Von Alvensleben, Amir Banaei-Esfahani, Laura A. Velazquez-Villegas, Karim Gariani, Melanie Korbelius, Maroun Bou Sleiman, Jéromine Imbach, Yu Sun, Xiaoxu Li, Alexis Bachmann, Ludger J.E. Goeminne, Hector Gallart-Ayala, Evan G. Williams, Julijana Ivanisevic, Johan Auwerx, and Kristina Schoonjans

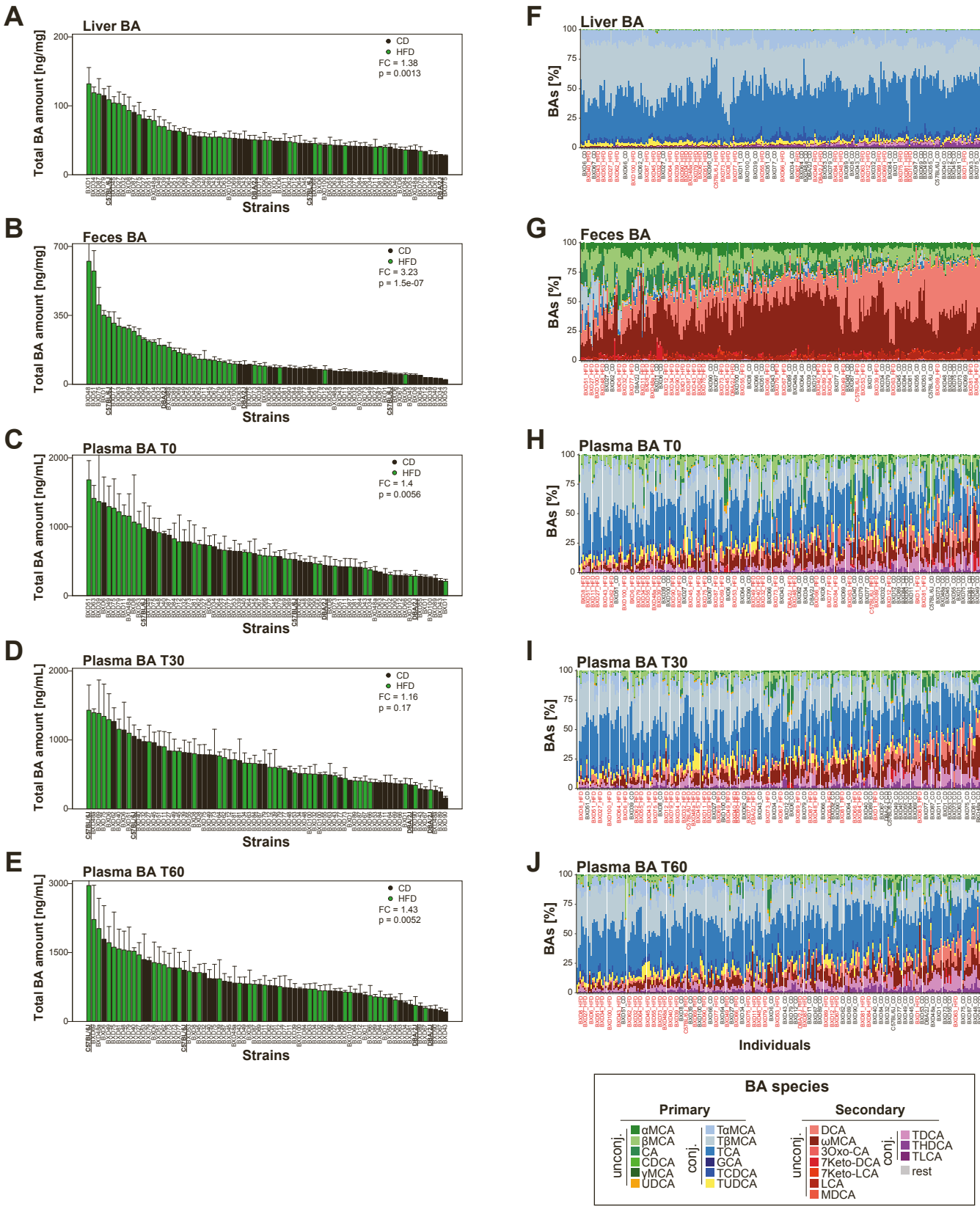

Figure S1. Related to Figure 2. Diversity of the BA composition and amount across strains and diets. (**A-E**) Barplots showing the BA amount in liver (**A**), feces (**B**), and plasma (**C-E**) of each BXD strain fed with either CD or HFD. Strains are ordered by the BA amount. Barplots are expressed as mean + SEM. P-values comparing strains fed with different diets were calculated using paired samples t-tests. Parental strains (C57BL/6J and DBA/2J) are indicated in bold and underlined. (**F-J**) Stacked barplots showing the BA composition (% of the BA amount in the various compartments at a given time) in liver, feces, and plasma (before and 30 or 60 minutes after gavage of a test meal) of each individual animal from different BXD strains. Animals were grouped by strain and diet, and ranked ordered by strain average of the proportion of total primary BAs. Strains fed a HFD are depicted in red. BA species are categorized and colored to highlight primary unconjugated (green and UDCA in orange), primary conjugated (blue and TUDCA in yellow), secondary unconjugated (red), and secondary conjugated (purple) BAs. The BA abbreviations are included in Table S1.

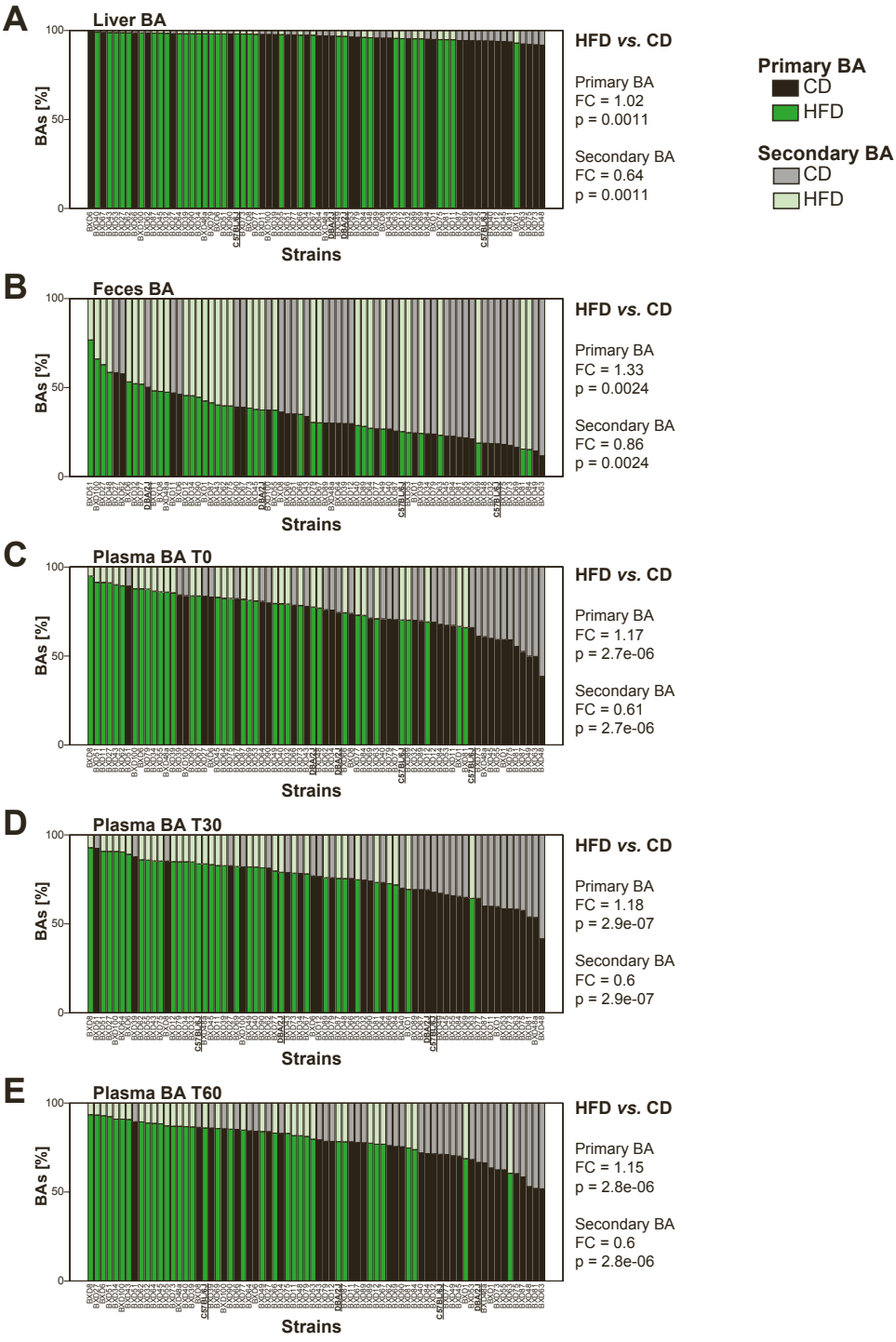

Figure S2. Related to Figure 2. The effects of diet on BA levels are influenced by the genetic background of the animals, the BA species, and the biological compartment. Barplots showing the percentage of primary (dark colors) and secondary (light colors) BAs in liver (**A**), feces (**B**), and plasma (**C-E**) of each BXD strain fed with either CD or HFD. Strains are ordered by the percentage of primary BA abundance over the total BA amount in the indicated biological compartment. Barplots are expressed as the averages of the animals in each strain. Fold changes (FC) were calculated between animals fed with HFD against those fed with CD. P-values comparing strains fed with different diets were calculated using paired samples t-tests.

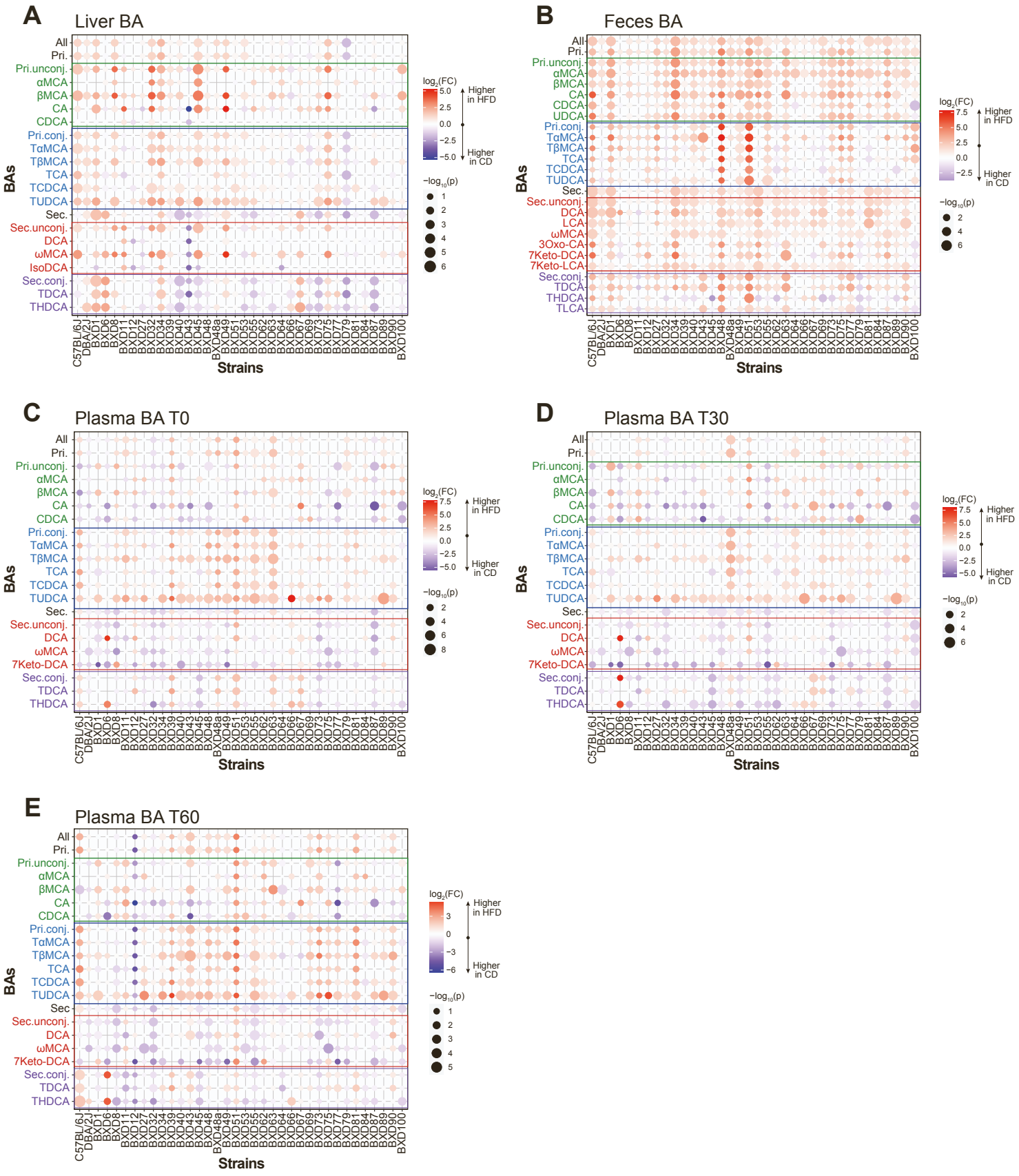

Figure S3. Related to Figure 2. The effects of diet on BA levels are influenced by the genetic background of the animals, the BA species, and the biological compartment. (**A-E**) Dot plots showing the BA level changes after HFD challenge in the liver (**A**), feces (**B**), and plasma (**C-E**) of each BXD strain. The dot color represents the fold change (FC) between the indicated BA levels in HFD versus CD, with red indicating higher in HFD and blue indicating higher in CD, and dot size refers to the significance of the changes. P-value was calculated using a two-tailed Student's t-test.

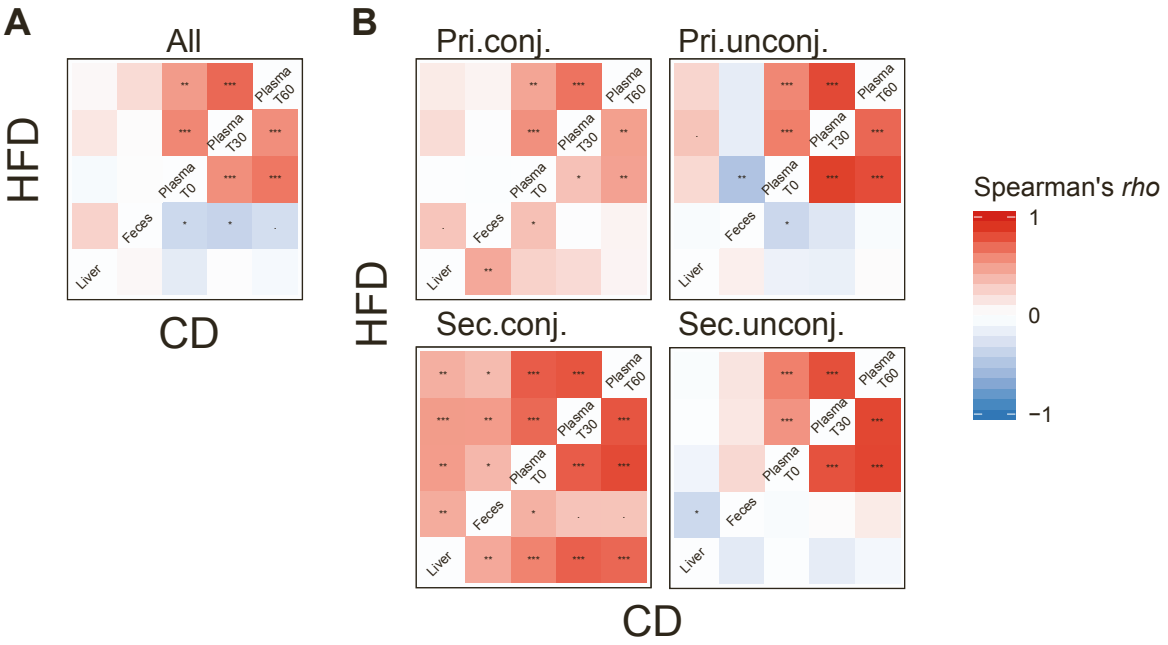

Figure S4. Related to Figure 2. Correlations between BA levels across different biological compartments and diets. Heatmap showing the correlations of the total BA amount (All) (**A**) or the sum of respective BA categories (**B**) between different compartments. Bottom right triangle of each heatmap is data from CD and top left triangle is data from HFD. Pri.conj., primary conjugated; Pri.unconj., primary unconjugated; Sec.conj., secondary conjugated; Sec.unconj., secondary unconjugated.

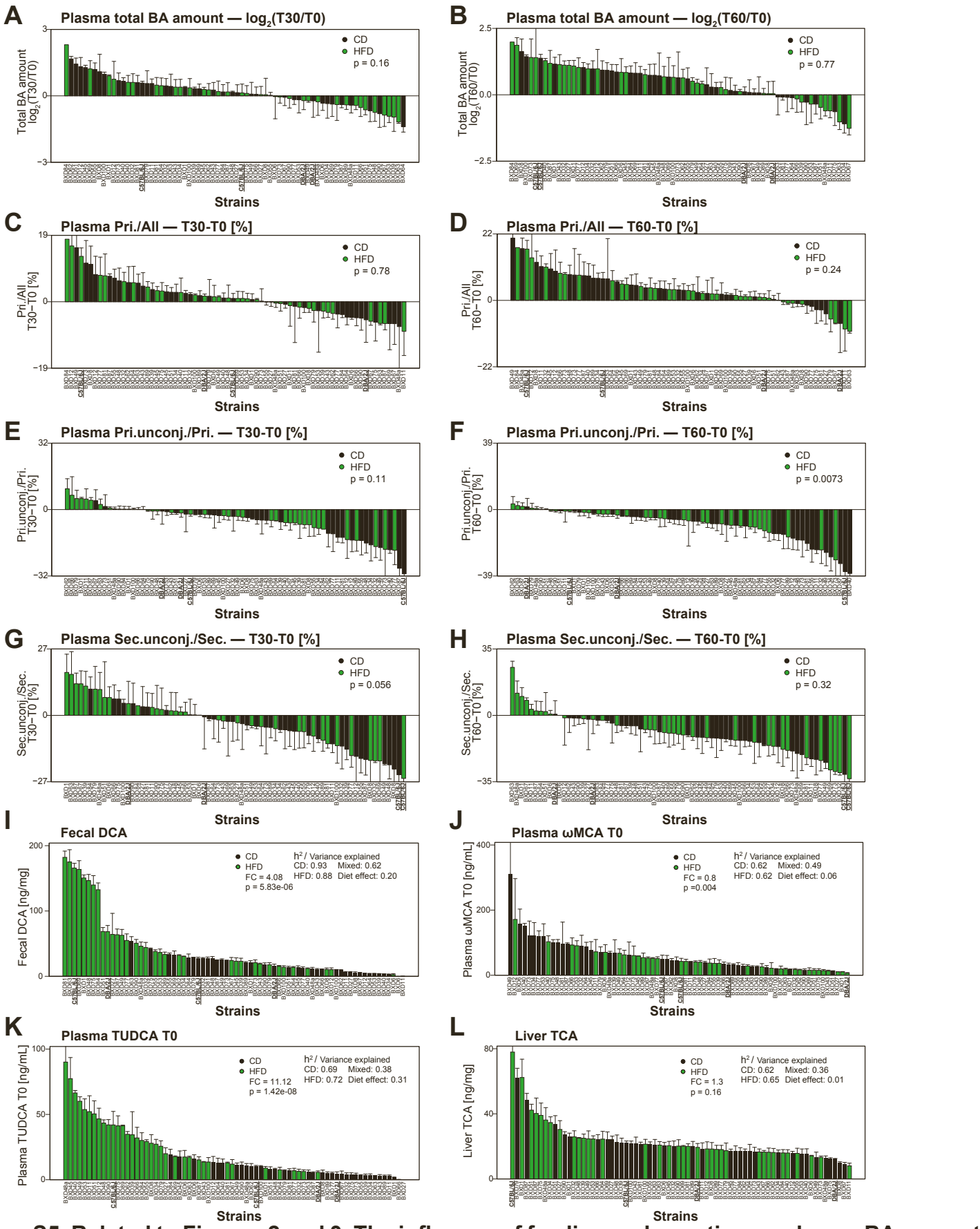

Figure S5. Related to Figures 2 and 3. The influence of feeding and genetics on plasma BA amount and conjugation. (**A-B**) The changes of plasma BA amount at 30 min (T30, **A**) or 60 min (T60, **B**) after test meal gavage compared to fasting levels (T0). (**C-D**) The changes of the ratio of plasma primary BAs to total BAs (Pri./All) at 30 min (T30, **C**) or 60 min (T60, **D**) after test meal gavage compared to fasting levels (T0). (**E-H**) The changes of the ratio of primary unconjugated BAs to primary BAs (Pri.unconj./Pri.) (**E-F**) or the ratio of secondary unconjugated BAs to secondary BAs (Sec.unconj./Sec.) (**G-H**) at 30 min (T30, **E**,**G**) or 60 min (T60, **F**,**H**) after test meal gavage compared to fasting levels (T0). (**I-L**) Barplots showing the levels of the same BAs (fecal DCA, plasma ωMCA T0, plasma TUDCA T0, hepatic TCA) represented in Figure 3B for each BXD strain. Strains are ordered by the respective BA levels. Barplots are expressed as mean + SEM. P-values were calculated using paired samples t-tests between CD and HFD. Fold change (FC) were calculated based on the average of BA changes in HFD compared to CD.

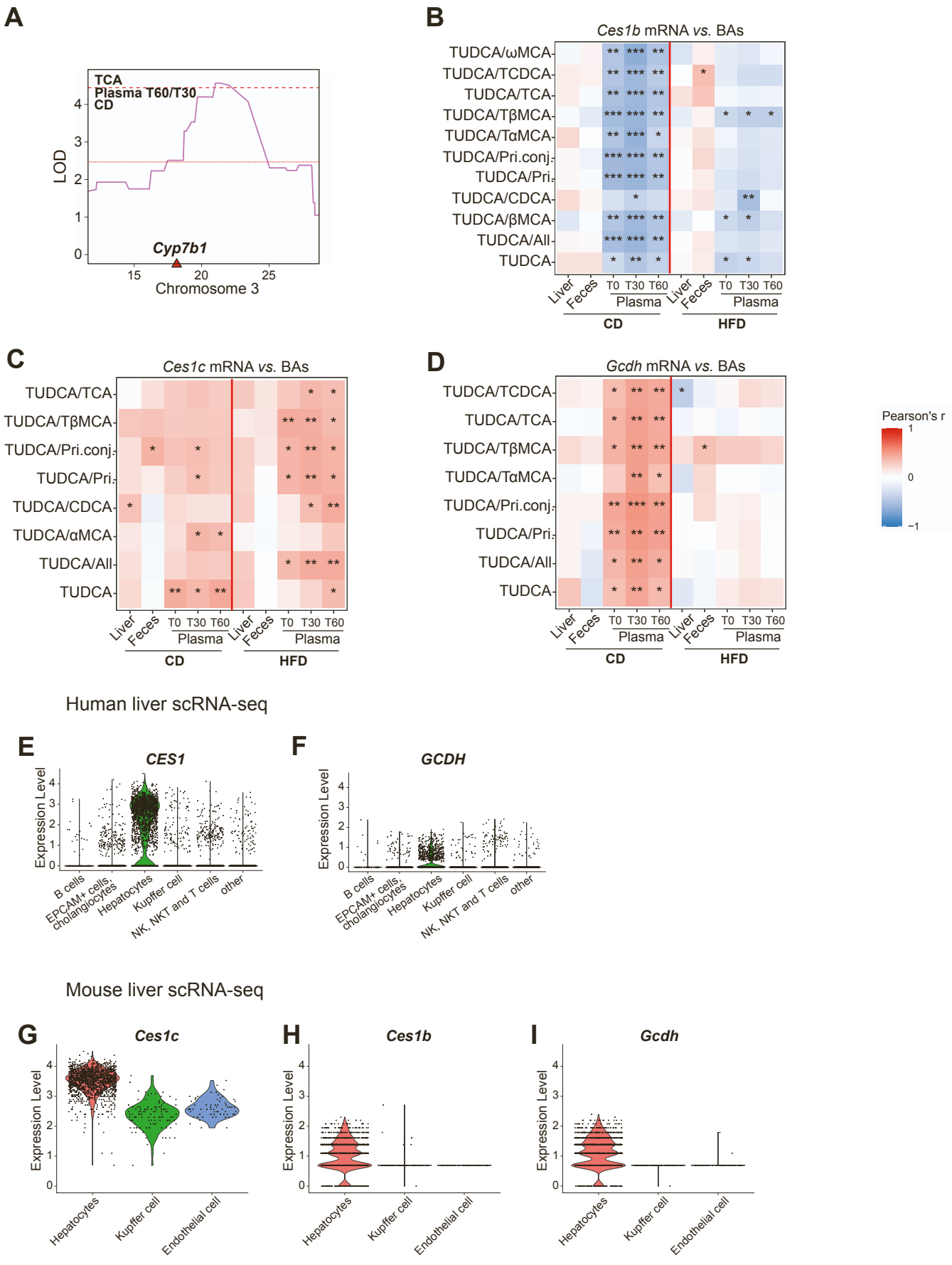

Figure S6. Related to Figures 5 and 6. Additional analysis of known and potential BA modulators. (**A**) Genetic position of the BA synthesis enzyme *Cyp7b1* on Chromosome 3 under the TCA QTL in plasma T60/plasma T30 in CD. (**B-D**) Heatmap representing the correlation between *Ces1b* (**B**), *Ces1c* (**C**), and *Gcdh* (**D**) hepatic mRNA expression and TUDCA levels in the indicated biological compartments. *p<0.05, **p<0.01, ***p<0.001. (**E-I**) Liver single-cell RNA-seq (scRNA-seq) data revealing the specific expression of *Ces1b*, *Ces1c* and *Gcdh* in hepatocytes. (**E-F**) Violin plots show the expression of for CES1 (**E**) and GCDH (**F**) across different cell types in human liver. (**G-I**) The expression of *Ces1c* (**G**), *Ces1b* (**H**), and *Gcdh* (**I**) across different cell types in mouse liver using violin plots.

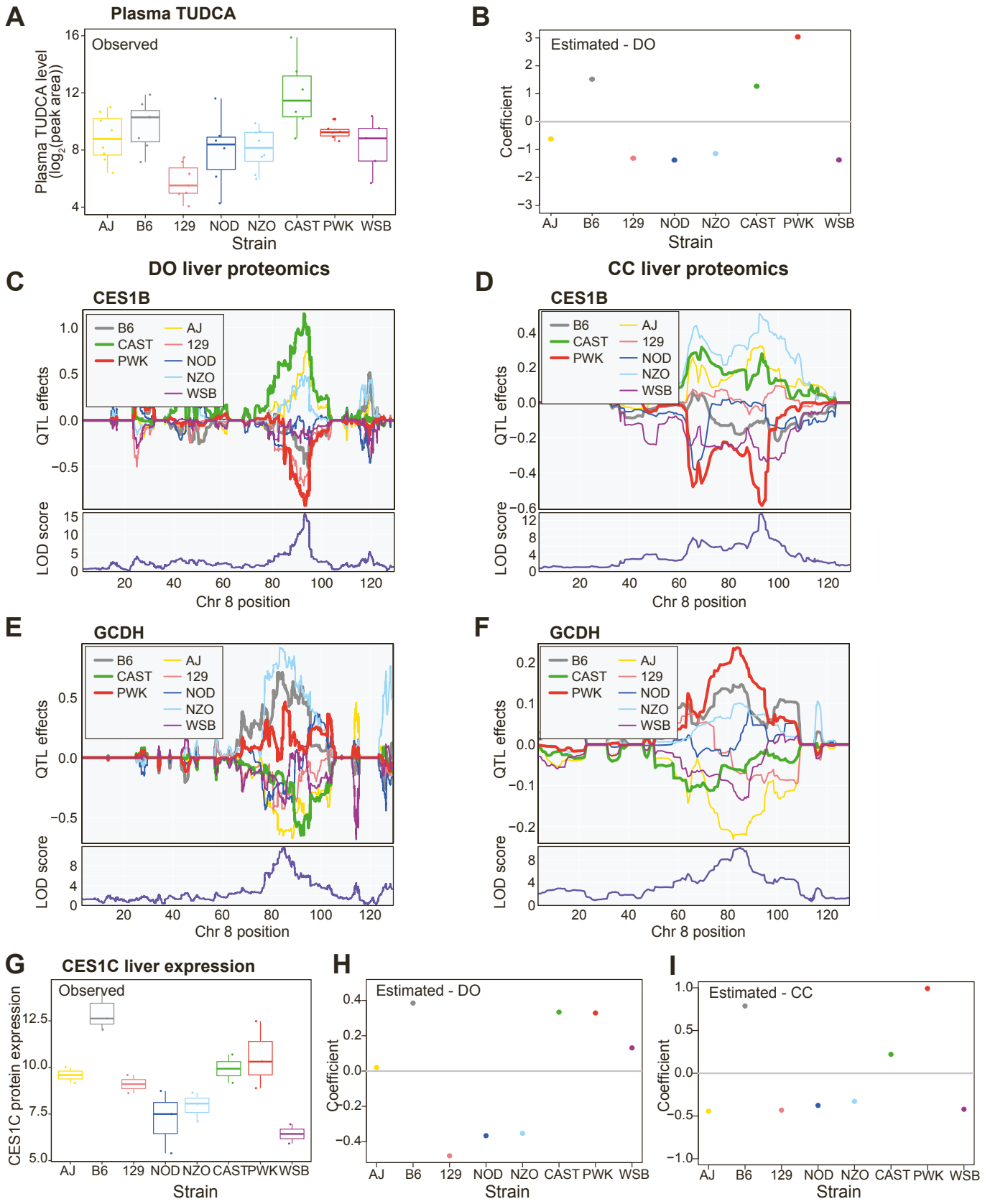

Figure S7. Related to Figure 7. Genetic effects of the QTL on plasma TUDCA levels in the DO animals and CC cohorts. (**A**) TUDCA levels (log_2 data) measured in the fasting plasma samples from male mice of the founder strains at 22 weeks of age. (**B**) Estimated coefficients of the founder strains haplotypes on plasma TUDCA levels for the TUDCA QTL on chromosome 8 in the DO mice, revealing the genetic effects of genotype alleles from each founder strain. (**C-I**) Haplotype effects and QTL results of CES1B (**C-D**) or GCDH (**E-F**) liver protein levels in DO (**C** and **E**) and CC (**D** and **F**) cohorts. For each plot, the x-axis indicates the genetic position on chromosome (Chr) 8. The y-axis for the top panel is the haplotype effects for the 8 founder strains, and the y-axis in the bottom panel is the LOD score. (**G**) CES1C liver protein levels measured from male mice of the founder strains at 26 weeks of age. (**H-I**) Estimated coefficients of the founder strains haplotypes on CES1C liver protein levels for the CES1C liver cis-pQTL on chromosome 8 in the DO (**H**) mice of 26 weeks of age and CC (**I**) mice of 8 weeks of age.

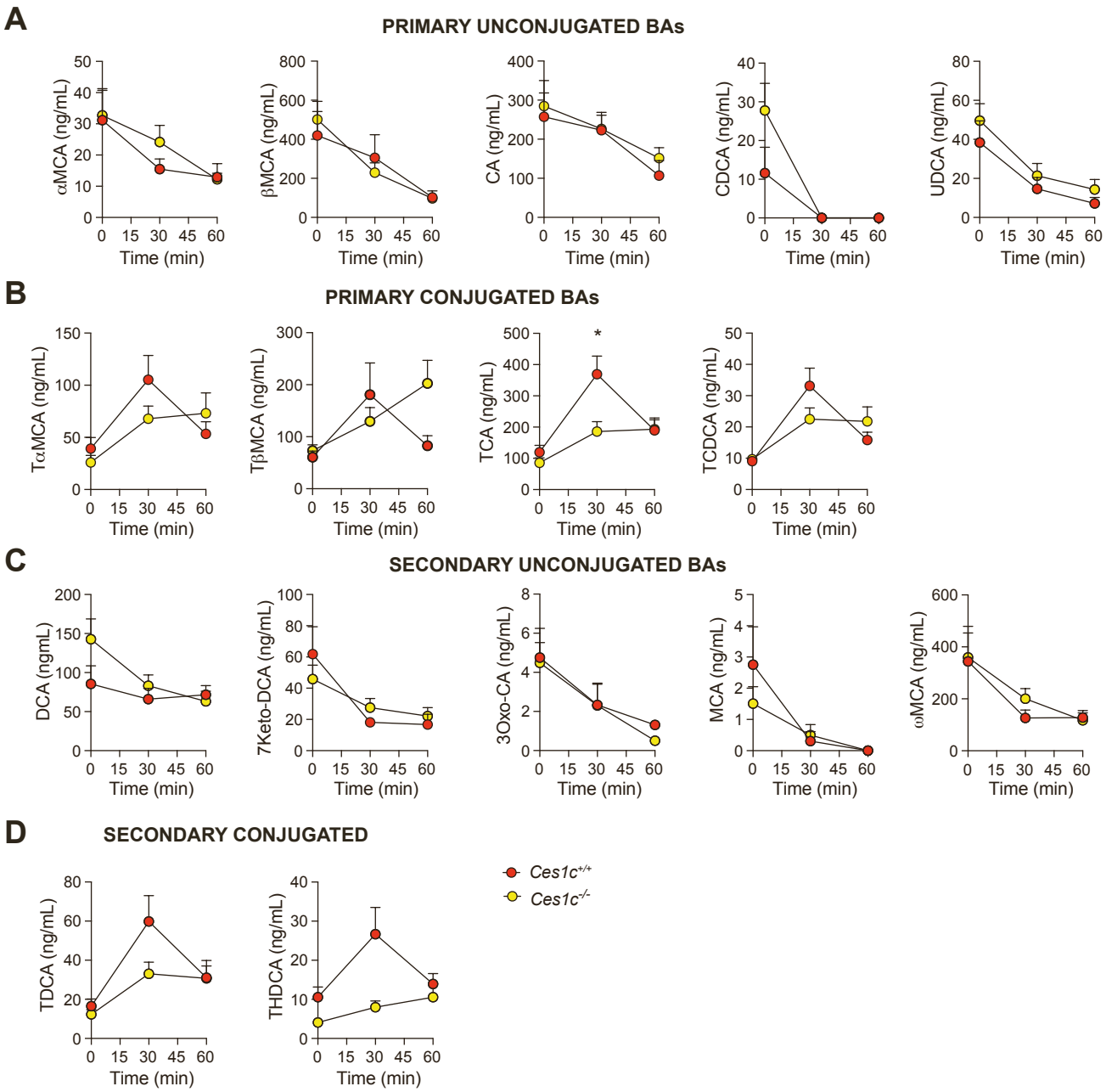

Figure S8. Related to Figure 7. Plasma BA levels in *Ces1c* wild-type and knock-out mice. (**A-D**) Primary unconjugated (**A**), primary conjugated (**B**), secondary unconjugated (**C**), secondary conjugated (**D**) BA levels in plasma in *Ces1c*$^{+/+}$ (n=9) and *Ces1c*$^{-/-}$ (n=11) male mice (20-week-old, fed CD – following the timeline in Figure 1A) before and 30 or 60 minutes after oral administration of a test meal. *p<0.05 vs. *Ces1c*$^{+/+}$ by two-way ANOVA followed by Bonferroni post-hoc test. Results are expressed as mean +SEM.

Table S1. List of the bile acids measured, their abbreviations, accurate m/z ratio, corresponding internal standards (used for quantification) and retention times (RT). Chromatographic resolution was essential for the separation of isobaric species.

Bile Acid	Abbreviation	H^- (m/z)	Internal Standard	RT min
Lithocholic acid	LCA	375.29047	d_4-LCA	20.6
7-Ketolithocholic acid	7Keto-LCA	389.26973	d_4-GDCA	15.5
Murocholic acid	MDCA	391.28538	d_4-CA	12.4
Ursodeoxycholic acid	UDCA	391.28538	d_4-GDCA	13.3
Chenodeoxycholic acid	CDCA	391.28538	d_4-CDCA	18.3
Deoxycholic acid	DCA	391.28538	d_4-DCA	18.5
Isodeoxycholic acid	isoDCA	391.28538	d_4-GDCA	19.7
3-Oxocholic acid	3Oxo-CA	405.26465	d_4-TCDCA	12.6
7-Ketodeoxycholic acid	7Keto-DCA	405.26465	d_4-GCA	11.0
α-Muricholic acid	α-MCA	407.28030	d_4-GCA	10.8
β-Muricholic acid	β-MCA	407.28030	d_4-GCA	11.2
ω-Muricholic acid	ω-MCA	407.28030	d_4-GCA	10.4
γ-Muricholic acid	MCA	407.28030	d_4-GCA	11.8
Cholic acid	CA	407.28030	d_4-CA	12.6
Glycolithocholic acid	GLCA	432.31193	d_4-GDCA	13.5
Glycoursodeoxycholic acid	GUDCA	448.30685	d_4-GCA	10.2
Glycohyodeoxycholic acid	GHDCA	448.30685	d_4-CA	10.6
Glycochenodeoxycholic acid	GCDCA	448.30685	d_4-GCDCA	12.9
Glycocholic acid	GCA	464.30176	d_4-GCA	10.3
Taurolithocholic acid	TLCA	482.29457	d_5-TLCA	13.0
Tauroursodeoxycholic acid	TUDCA	498.28948	d_4-TCA	5.1
Taurohyodeoxycholic acid	THDCA	498.28948	d_4-TCDCA	5.5
Taurochenodeoxycholic acid	TCDCA	498.28948	d_4-TCDCA	10.6
Taurodeoxycholic acid	TDCA	498.28948	d_5-TDCA	10.9
Tauro-α-muricholic acid	TαMCA	514.28440	d_4-TαMCA	2.1
Tauro-β-muricholic acid	TβMCA	514.28440	d_4-TβMCA	2.3
Taurocholic acid	TCA	514.28440	d_4-TCA	5.8